The changing strength of carbonate silt: Parallel penetrometer and foundation tests with cyclic loading and reconsolidation periods

Z. Zhou, D.J. White and C.D. O'Loughlin

Zefeng ZHOU (corresponding author)
Centre for Offshore Foundation Systems and ARC Research Hub for Offshore Floating Facilities
University of Western Australia
Perth, WA 6009, Australia
Tel: +61 403848151
Email: zefeng.zhou@research.uwa.edu.au

DNV GL
Veritasveien 1, 1363 Høvik, Norway.
Tel: +47 46884140
Email: zefeng.zhou@dnvgl.com

David J. WHITE
University of Southampton and ARC Research Hub for Offshore Floating Facilities
Southampton, Southampton SO17 1BJ, UK
Tel: +44 23 8059 6859
Email: david.white@soton.ac.uk

Conleth D. O'LOUGHLIN
Centre for Offshore Foundation Systems and ARC Research Hub for Offshore Floating Facilities
University of Western Australia
Perth, WA 6009, Australia
Tel: +61 8 6488 7326
Email: conleth.oloughlin@uwa.edu.au

Number of words (excluding the abstract, list of notation, acknowledgements, references, tables and figure captions): 7234
Number of tables (excluding appendix): 6
Number of figures (excluding appendix): 18

ABSTRACT

This paper describes a centrifuge study using novel penetrometer tests (T-bar and piezoball) and model foundation tests to explore through-life changes in the strength of a reconstituted natural carbonate silt. The test procedures include episodic cyclic loading, which involves intervals of pore pressure dissipation between cyclic packets. These loads and the associated remoulding and reconsolidation cause significant changes in the soil strength and foundation capacity. Soil strength changes from penetrometer tests differed by a factor of 15 from the fully remoulded strength to a limiting upper value after long-term cyclic loading and reconsolidation. For the model foundation tests, the foundation capacity of a surface foundation and a deep-embedded plate were studied. The soil strength interpreted from the measured foundation capacity varied by a factor of up to three due to episodes of loading and consolidation, with an associated order of magnitude increase in the coefficient of consolidation. The results show a remarkable rise in soil strength over the loading events, and provide a potential link between changes in soil strength observed in penetrometer tests and the capacity of foundations, allowing the effects of cyclic loading and consolidation to be predicted.

Keywords: carbonate silt, penetrometers, model foundation, changing soil strength, foundation capacity, cyclic loading and reconsolidation.

1. INTRODUCTION

Many offshore foundations are subjected to intermittent episodes of cyclic loading, or remoulding, and reconsolidation during their installation and long-term operation. The cyclic loading and reconsolidation processes cause changes in foundation capacity. To assess these changes, it is necessary to estimate the changes in the strength of the surrounding soil.

The weakening effect of cyclic loading on soil strength is well recognized throughout design practice, and methodologies for determining the cyclic 'fatigue' of soil during undrained cyclic loading are well established (e.g. Andersen et al. 1988; Andersen 2015). On the other hand, the effect of consolidation on soil strength can be very important and beneficial for design practice, or can introduce additional criticalities. For instance, during footing installations for mobile offshore drillings rigs, periods of consolidation are encountered due to weather and other delays, or deliberate waiting periods are used to enhance the foundation capacity. Through a consolidation period, the recovery of soil strength enhances the soil penetration resistance, which may raise the capacity to an acceptable level that would enhance the range of wave conditions in which the jack-up can safely operate, or may heighten the risk of spudcan punch-through (e.g. Purwana et al. 2005; Bienen and Cassidy 2013; Amodio et al. 2015; Wang and Bienen 2016; Ragni et al. 2016).

Similarly, all subsea foundations and anchoring systems are subjected to low levels of cyclic loading throughout their life, either from day-to-day cycles of operating temperature, from mild sea states or changes in vessel condition. These cyclic episodes are sustained over a significantly longer period than a single storm and may progressively strengthen the surrounding soft soil through drainage and consolidation. For subsea facilities, where the dominant design action is from thermal expansion effects rather than storm loading, the changing capacity through life is important. These foundations are sometimes designed to fail in sliding to relieve expansion loads, so a gain in capacity may be unwanted. Or, the design expansion loads may only build up slowly during the operating life. In this case, the rise in foundation capacity may outpace the increasing design load.

The most common design approach to achieve a target reliability of an offshore foundation is via load and resistance (or material) factors, which are applied to characteristic design values (e.g. DNV GL 2018a, b; API 2005; ISO 2014). For anchors or shallow foundations on soft clay, the partial safety factors are usually determined through a reliability analysis that accounts for variability in load and material properties, model error and design situations. The partial factors

are calibrated to target probabilities of failure for different failure consequences (i.e. 10^{-4} for CC1 and 10^{-5} for CC2 recommended in DNV GL RP E301 and E302).

Currently, for offshore shallow foundations and anchors, the basis for the partial factors in the standards ignores the effects of consolidation. As a result, the reliability is underestimated if a mechanism of increasing strength, such as the consolidation process considered in this paper, is present.

Reliability-based approaches can however be enhanced to allow a change in capacity over the operating life of a foundation to be incorporated in design. It may be possible to verify that a foundation has adequate through-life reliability even if the material factor is marginally inadequate during early life, because of a larger margin of safety in later life. Such an approach is similar to the current use of less onerous design conditions during temporary operations for installation and hook up.

Experimental studies (Lehane and Jardine 2003; Lehane and Gaudin 2005; Bienen and Cassidy 2013; Fu et al. 2015; Li et al. 2015; Cocjin et al. 2017) indicate an increase in the capacity of foundations due to sustained load and consolidation. Numerical analyses using the modified Cam Clay (MCC) model match these trends (Bransby 2002; Zdravkovic et al. 2003; Feng and Gourvenec 2015; Wang and Bienen 2016). Based on the studies, Gourvenec et al. (2014, 2017) set out a simple method using a 'lumped' value of changing soil strength to predict the changes in capacity of a shallow foundation due to sustained load with degree of consolidation.

The present study extends this prior work to consider the effects of cyclic loading and consolidation on soil strength using penetrometers and foundation model tests.

2. EXPERIMENTAL PROGRAMME

2.1 UWA geotechnical beam centrifuge

The tests were performed at the University of Western Australia using the fixed beam geotechnical centrifuge that has a nominal radius of 1.8 m (Randolph et al. 1991). All the tests presented in this paper were carried out at an acceleration level of 100g. The soil sample was set up in a rectangular 'strongbox', which has dimensions of 650 × 390 mm in plan and is 325 mm deep. An actuator was used to impose vertical and horizontal movements on the model. Load- or displacement-controlled operation is achieved with a software feedback loop using the output of a load cell or displacement transducer. Data acquisition used a high-speed Ethernet-based system with data streaming in real time to a remote desktop (Gaudin et al.,

2009).

2.2 Test instrumentation

2.2.1 Model foundation

A simple circular foundation model with a diameter, D_f = 40 mm, and with a thickness, t_f = 10 mm was used in this study. The model, as illustrated in Figure 1a, was fabricated from aluminium and connected to a cylindrical shaft with a diameter of 10 mm. The base of the model foundation was equipped with a pore pressure transducer (PPT) to monitor the excess pore pressure during installation and cyclic loading, and subsequent dissipation. A vertically-oriented load cell with a measurement range of 2 kN was connected directly to the foundation shaft to measure the applied vertical foundation-soil load, while a bending arm with a measurement range of 60 Nm was positioned in-line with the load cell to measure the horizontal load applied to the foundation. The experimental setup of the footing test is presented in Figure 2a.

2.2.2 Penetrometers

The penetrometer tests were carried out using a model scale T-bar (Stewart and Randolph 1991) and a model scale piezoball (Mahmoodzadeh and Randolph 2014) (Figure 1b). The dimensions and instrumentation of these penetrometers are detailed in Table 1. They were fabricated from aluminium with a load cell located just above the bar or sphere to minimize the measurement error due to shaft friction. The piezoball featured pore pressure measurement at the mid-face position, half the radius vertically above the tip of the ball. The experimental setup of the penetrometer test is presented in the Figure 2b.

2.3 Soil sample preparation

The soil sample was prepared by reconstituting a natural carbonate silt retrieved from offshore Australia at a targeted water content of 145%. The slurry was mixed continuously for ~48 hours and then poured slowly into the centrifuge strongbox. A 10 mm layer of sand was placed at the base of the strongbox (i.e. before pouring the slurry) and overlayed by a geosynthetic drainage layer. The sample was consolidated under self-weight in the centrifuge at an acceleration of 100 g for 5 days, with an approximately 30 mins pause towards the end of the first day during which time additional slurry was added to ensure that the final sample height was approximately 235 mm. A ~35 mm water layer was maintained above the soil sample during the subsequent testing.

Geotechnical properties of the carbonate silt as determined from a set of laboratory tests are presented in Table 2.

2.4 Soil characterization

2.4.1 Undrained shear strength

A set of 'conventional' T-bar tests (Stewart and Randolph 1991) was performed to measure profiles of the initial undrained shear strength, $s_{u,i}$, and the fully remoulded shear strength, $s_{u,rem}$, at intervals over the testing period. The tests involved monotonic penetration and extraction, as well as a cyclic phase at a model depth of 165 mm ($z/D_{T\text{-}bar}$ = 33). The cyclic phase involved 20 cycles (a cycle defined as both penetration and extraction) with a cyclic amplitude of 30 mm ($6D_{T\text{-}bar}$). Both the monotonic and cyclic phases employed the same penetration (and extraction) velocity, v_p = 3 mm/s (at model scale). This was sufficient to ensure undrained conditions, noting that the dimensionless group, $v_p d_e/c_h$ = 33 (where d_e = 11.3 mm, is the equivalent diameter of the T-bar, defined as the diameter of a circle with the same area as the T-bar, and c_h is the coefficient of horizontal consolidation, taken as 32 m^2/yr, as discussed later in the paper), in excess of the $v_p D/c_h > 10$ criteria for undrained behaviour (e.g. House et al. 2001; Randolph and Hope 2004; DeJong and Randolph 2012).

The results of the T-bar tests near the beginning and end of the eight-day testing program are presented in Figure 3. Figure 3a plots the undrained shear strength with normalised depth, $z/D_{T\text{-}bar}$, where $s_u = q_{T\text{-}bar}/N_{T\text{-}bar}$ was interpreted assuming a constant T-bar capacity factor of $N_{T\text{-}bar}$ = 10.5. This value was selected based on theoretical solutions (Einav and Randolph 2005; Martin and Randolph 2006), and it has been adopted for other studies using the same soil (Chow et al. 2019; Chang et al. 2019; Zhou et al. 2019b; O'Loughlin et al. 2019). Negative values of undrained shear strength correspond to a downwards soil resistance on the T-bar penetrometer, which is created when the penetrometer moves upwards. The undrained shear strength profile can be simplified as linear profiles with a zero mudline strength given by

$$s_{u,i} = kz \tag{1}$$

where k is the strength gradient, $k = s_{u,i}/z$ using depth, z, in the equivalent prototype scale. The average strength gradient on Figure 3a is k = 4 kPa/m, which is higher than expected for this soil (and inconsistent with the strength ratio measured in other centrifuge samples and element tests on the same soil, reported in Chow et. al. 2019). This is because the tests reported here were affected by steady downward seepage through the sample, which may be attributed to a leak in the drainage pipe (shown in Figure 2) and occurred over the course of the tests. The

steady seepage increases the profile of vertical effective stress with depth. Other studies using the same soil, reconstituted in the same way but without the seepage problem, show a strength of gradient of 2 kPa/m (Chow et al. 2019; Zhou et al. 2019b; O'Loughlin et al. 2019), which is half of the gradient recorded in this study. Therefore, all the present results have been interpreted considering a doubling of the geostatic effective stress profile. This is equivalent to either a doubling of the effective unit weight or the g-level (N_g = 200).

In the T-bar test, the remoulding process causes degradation of the undrained shear strength until the fully remoulded condition is reached. A strength variation ratio is defined as $s_{u,cyc}/s_{u,i}$ where $s_{u,cyc}$ is the degrading undrained strength during the cyclic phase and $s_{u,i}$ is the initial undrained shear strength measured in the first penetration. The evolution of this ratio at a depth of $z/D_{T\text{-}bar}$ = 33, is plotted in Figure 3b. For each T-bar test, the final value of $s_{u,cyc}/s_{u,i}$ indicates the soil sensitivity, S_t, where S_t is the ratio between the initial strength and the fully remoulded undrained shear strength. The sensitivity interpreted from the T-bar tests is $S_t \sim 5$.

2.4.2 Consolidation characteristics

The coefficient of horizontal consolidation, c_h of the carbonate silt was determined from piezocone dissipation tests conducted at various penetration depths in centrifuge tests reported in Chow et al. (2019). Dissipations were interpreted using the Teh and Houlsby (1991) theoretical solution. The resulting variation in c_h with vertical effective stress is shown in Figure 4 (where the vertical effective stress was calculated using an effective unit weight, γ' = 5.5 kN/m^3, taken as the average γ' from moisture content determinations made on sample cores taken after testing). Figure 4 also includes values of c_h interpreted from an episodic piezoball test (described later) using the Mahmoodzadeh et al. (2015) numerical solution. c_h from the piezocone tests (or estimated by 2 × Equation 2) is ~25% greater than c_h from the piezoball , which is broadly consistent with the 33% difference reported by Colreavy et al. (2016).

Figure 4 also shows the coefficient of vertical consolidation, c_v, as measured in Rowe cell consolidation tests at effective vertical stress levels, σ'_v = 15 to 120 kPa. The coefficient of vertical consolidation, c_v, increases with vertical stress level, and can be expressed as

$$c_v = (1.17\sigma'_v)^{0.5} \quad (2)$$

using units of kPa for σ'_v and m^2/year for c_v. Using Equation 2, the dependence of c_v on σ'_v is well captured (Figure 4). Scaling from Equation 2 by a factor of 2 provides a reasonable estimation of c_h values from the piezocone tests, allowing $c_h/c_v \sim 2$ to be inferred for this soil.

2.5 Test programme

The test programme included penetrometer tests and model foundation tests, as summarized in Table 3. Test locations within the strongbox are shown in Figure 2c. A minimum (centre-to-centre) distance of 190 mm ($4.75D_f$) was allowed between adjacent foundation tests, and the minimum distance between the centre of the foundation and the strongbox walls was 110 mm ($2.75D_f$), such that interaction and boundary effects may be considered negligible (Stanier et al. 2014; Wang and Bienen 2016). The penetrometer tests were episodic – one using a T-bar and one using a piezoball – with cyclic stages interspersed with a reconsolidation period. The test stages and results are presented in Section 3.

The model foundation tests were divided into two types: surface foundation sliding and embedded plate penetration and extraction. The purpose of the tests was to investigate changes in foundation capacity over a period and loading history that represents (in a simplified way) foundation installation through long-term operation. The test stages and results are presented in Section 4.

3. PENETROMETER TESTS: CHANGING SOIL STRENGTH

3.1 Test procedures

The episodic T-bar test involved cycles of penetration and full extraction with a consolidation period of 780 s between each cycle (representing 0.25 years in prototype scale). The T-bar was positioned above the mudline during the consolidation period. As illustrated in Figure 5a, each cycle constitutes penetration and extraction to a depth of $36D_{T\text{-}bar}$. As is customary (Einav and Randolph 2005) – and used earlier in Figure 3b – a single penetration or extraction represents an incremental cycle number of $\Delta N = 0.5$, such that the T-bar test starts from a cycle number, $N = 0.5$ for initial penetration and $N = 1.0$ during first extraction. A total 78 cycles were carried out during the test. Penetration and extraction was conducted at the same 3 mm/s velocity used in the conventional T-bar test, which (as described earlier) is sufficient for undrained conditions during the movement. The total duration of the test was ~19 hours at model scale.

The episodic cyclic piezoball test differed from the episodic T-bar test in that each cyclic phase involved a full set of 20 cycles, which (as will be shown later) was sufficient to fully remould the soil, since it is more than a recommended 10 cycles to fully remould soil strength for a cyclic ball test (Einav and Randolph 2005; Zhou and Randolph 2009). The test involved two phases, at depths of $4D_{PB}$ and $10.5D_{PB}$, with similar procedures in each phase (see Figure 5b):

1. The piezoball was penetrated to the testing depth at v_p = 1 mm/s ($V' = v_p D_{PB}/c_v$ = 118) which enables an undrained condition.
2. The piezoball was held at this depth for an initial consolidation period.
3. Three episodes of 20 cycles were performed around each depth after the initial consolidation. In each cycle, the ball was penetrated with a cyclic amplitude of $\pm 1.5D_{PB}$, except that the initial downward half-cycle penetrated a further 1D beyond the main cyclic range. This is usual practice in cyclic penetrometer tests to eliminate end effects within the pattern of cyclic resistance. A one-hour consolidation period was permitted between each cyclic episode.

3.2 Test results and discussion

3.2.1 Episodic T-bar test: single cycles interspersed with reconsolidation

Selected strength profiles from the 78 cycles are presented in Figure 6. The undrained shear strength is determined from the measured penetration resistance, $q_{T\text{-}bar}$, as $s_u = q_{T\text{-}bar}/N_{T\text{-}bar}$, where a capacity factor of 10.5 is used (Martin and Randolph 2006).

The duration of the cyclic phase means that some pore pressure from the initial cycles can dissipate by the time the 20th cycle is complete. However, the trend of continuous reduction in resistance during the 20 cycles shows that the changing strength is dominated by remoulding and pore pressure generation, rather than consolidation (Figure 3). It is possible, however, that a slightly lower remoulded strength would be observed if the cycles were faster, and therefore closer to fully undrained.

Owing to the 'breaking-surface' cycling, a trench developed with a shape of a deep slot in the centre of a wide bowl at the penetrometer location (see Figure 7). This created a successively lower touchdown point as the mudline level changed. In Figure 7a, the trench depth increased with cycle number, reaching a depth of $4D_{T\text{-}bar}$ after N = 20, before increasing (at a higher rate) to ~$20D_{T\text{-}bar}$ after N = 60 cycles. The initial trench formation to about 4 times the T-bar diameter is due to the high strength ratio ($s_u/\gamma' D_{T\text{-}bar}$) in this carbonate silt, and therefore the deeper depth that can develop prior to soil flowing around the T-bar (White et al. 2010). The continued deepening of the trench is due to the gradual reduction in specific volume of the penetrated column of soil due to consolidation. In a similar episodic T-bar test in kaolin clay (Cocjin et al. 2014), the lower strength ratio of kaolin led to a shallower trench depth of ~ $2D_{T\text{-}bar}$ after 60 cycles. Therefore, no resistance and therefore soil strength information was available for this

shallow zone in later cycles.

However, the changing strength can be indicated by the evolution of the strength gradient, k defined as a ratio of $\triangle s_u$ to $\triangle z$, over a particular depth range, chosen here as between $z/D_{T\text{-}bar}$ = 30 and $z/D_{T\text{-}bar}$ = 35. This eliminated the effect of the lowering touchdown point and also the sharp increase in penetration resistance at the bottom limit of the penetration, where the penetration resistance 'sensed' the stronger underlying sand and the rigid base of the strongbox. The strength gradient ratio, k_{cyc}/k_i, inferred over this range is presented in Figure 8.

After an initial reduction, reflecting the remoulding process, the strength gradient increases as the remoulding is eclipsed by reconsolidation effects. The enhanced soil strength gradient after 40 cycles approaches a stable value that is about three times the strength gradient measured during the first penetration, i.e. $k_{cyc}/k_i \approx 3$.

Figure 8 also includes results from a similar episodic T-bar test in kaolin clay (Cocjin et al. 2014) to provide context for such tests in other soils. The strength gradient factor picked up between $z/D_{T\text{-}bar}$ = 5 and $z/D_{T\text{-}bar}$ = 6.5 (and also the strength ratio, $s_{u,cyc}/s_{u,i}$, at a specified normalised depth of $z/D_{T\text{-}bar}$ = 8 – given in Cocjin et al. 2014) show a similar cyclic variation for both soil types, converging to a long term limit of ~3 times the initial value.

In summary, for both soils, which are initially normally-consolidated, the long term undrained strength after many cycles of remoulding and reconsolidation is three times greater than the initial undrained strength.

3.2.2 Episodic cyclic piezoball test: multiple (20) cycles interspersed with reconsolidation

The results of the piezoball test are expressed in terms of a ball penetration resistance, q_{PB}. The penetration resistance has also been converted to soil strength via a capacity factor of N_{ball} = 11, chosen as it gives the same undrained strength as the T-bar test, and is also consistent with the literature (Low et al. 2010; DeJong et al. 2010).

Before the cyclic loading was applied, the piezoball was held at each testing depth for an initial consolidation period, sufficient for full dissipation of the excess pore pressure measured at the mid-face location on the ball (shown in Figure 9). The consolidation periods were:

- 1.5 hrs model scale, $T \sim c_h t/D_{PB}^2$ = 10.5 in phase 1 (c_h = 14 m^2/year), at z/D_{PB} = 4,
- 2.5 hrs model scale, $T \sim 29$ in phase 2 (c_h = 24.5 m^2/year), at z/D_{PB} = 10.5.

The resulting profiles of undrained shear strength at the two testing depths are presented in

Figure 10a and b for the first phase (at $4D_{PB}$), and Figure 10c and d for the second phase (at $10.5D_{PB}$), respectively. The initial full consolidation period at the testing depth caused a significant gain in penetration resistance, to values of ~1.5 and ~1.8 times the corresponding initial soil strength at $4D_{PB}$ and $10.5D_{PB}$, respectively.

A strength variation ratio, $s_{u,cyc}/s_{u,i}$ at two depths, $4D_{PB}$ (Figure 10b) and $10.5D_{PB}$ (Figure 10d) shows the variation in soil strength. Within each episode, soil strength declines rapidly in the first few cycles until a steady limit is reached, which represents a fully remoulded state. The reduction in $s_{u,cyc}/s_{u,i}$ during each episode (and at the two depths) is typically ~5, consistent with the soil sensitivity derived from the T-bar tests in Figure 3b. A regain in soil strength follows each reconsolidation process, and the fully remoulded strength also increases.

4. FOUNDATION TESTS: CHANGING FOUNDATION CAPACITY

4.1 Test procedures

The first set of model foundation tests involved three horizontally-loaded surface foundation tests. The procedures followed in each test are set out in Table 4. For each test, the installation of the model foundation was achieved by driving the vertical axis of the actuator at a slow rate of 0.1mm/s until the target vertical compression resistance (v_{op} ~ 22.5 kPa) was recorded by the load cell, immediately followed by unloading to $2/3v_{op}$. This value was maintained throughout the test including the failure stage (representing self-weight loading, shown in Figure 11a). In test 1 the model foundation was immediately loaded to failure by horizontal displacement control at 0.1 mm/s after installation, while an initial consolidation was allowed in tests 2 and 3. In test 3, 10 cycles of horizontal loading and consolidation were applied after the initial consolidation (Figure 11b), in which the episodic cycles involved sustained load alternating between 75% and -75% of h_{cu}, where h_{cu} is the consolidated undrained horizontal capacity (described later). Finally the foundation was loaded horizontally in 0.1 mm/s to measure the cyclic consolidated undrained horizontal capacity, $h_{cu,cyc}$.

The second set of model foundation tests involved vertical penetration and extraction of a buried plate foundation with a hierarchy of imposed loads and consolidation events similar to the first set, and shown in Figure 11c. The procedures followed in each test are set out in Table 5. Each test involved installation at v_p = 0.1 mm/s (such that v_pD_f/c_h = 21 and the response may be considered undrained; House and Randolph 2001) to a depth of w/D_f ~ 3.5 followed by consolidation under either sustained monotonic load (~ 75% v_{uu} in test 4 or ~ 75% $v_{uu,tens}$ in test 6, where v_{uu} and $v_{uu,tens}$ are undrained unconsolidated foundation capacity measured during

initial penetration or extraction, respectively) or episodic cyclic load (10 cycles) in which the episodic cycles involved sustained load alternating between ~10% and ~75% of v_{uu} (test 5) or $v_{uu,tens}$ (test 7). The penetration depth $w/D_f = 3.5D_f$ was selected to ensure that a deep failure mechanism developed (Hossain et al. 2005; Hossain and Randolph 2009) and that the test was unaffected by potential shallow embedment effects or water entrainment. Then, in either compression or tension, the model foundation was loaded in displacement control at 0.1 mm/s to failure in the same direction. For the tension tests, the plate was penetrated to a greater depth (~$4.5D_f$) initially, before being pulled up to the position of the sustained loading tests.

4.2 Results and discussion

This section presents the results of the foundation model tests, firstly for the horizontally-loaded surface foundation, and secondly for the vertically-loaded plate. For each foundation type, the first test quantifies the undrained foundation capacity for the initial soil strength conditions. This is defined as the 'unconsolidated undrained' (UU) foundation capacity. In the other tests, the foundation is subjected to a series of loads, and then the foundation was loaded monotonically until beyond the occurrence of a clearly defined peak resistance or a displacement of 0.6 times the foundation diameter. The foundation capacity is then identified as the peak resistance for Test 2 and 3 and the resistance at $0.33D_a$ (equivalent to the mobilisation to the peak resistance in Test 3) for Test 1. The foundation capacity in these tests is compared with the base case UU test and the relative change in foundation capacity is identified, equivalent to the strength variation ratio defined in the penetrometer testing.

In addition, an attempt is made to back-calculate the operative soil strength at failure, making reasonable assumptions where needed. The purpose is to establish the changing strength of the soil around the foundation, as well as simply the changing foundation capacity, and compare these observations with the changes identified during the penetrometer tests.

The key results are summarized in Table 6. For the horizontally-loaded surface foundation, the foundation capacity is denoted, $h = H/A_{base}$, where H is the horizontal load at failure. For the embedded plate, the foundation capacity is denoted, $v = V/A_{base}$, where V is the vertical load applied to the plate at failure. In both cases, A_{base} is the base area of the foundation, $A_{base} = \pi D_f^2/4$ ($A_{base} \sim 0.00126$ m^2 with the diameter of the model foundation, $D_f = 40$ mm). The base case UU capacities are denoted h_{uu}, v_{uu} and v_{uu_tens}. The additional subscripts that represent the other loading histories are introduced with each individual test in the following sections.

4.2.1 Model foundation tests: shallow foundation under horizontal load

The variation of horizontal resistance with normalized horizontal foundation displacement, u/D_f, is presented in Figure 12a, and the foundation trajectory during the loading to failure is shown in Figure 12b. The tests are discussed individually in the following sub-sections.

4.2.1.1 Test 1: Unconsolidated-undrained capacity (h_{uu})

During the failure stages of Test 1, the mobilized horizontal resistance increases with horizontal displacement at a steady rate over the majority of the sliding movement. This increase may be linked to the soil berm growing ahead of the foundation. The value of h_{uu} is defined at a normalized sliding displacement, $u/D_f \sim 0.33$, as $h_{uu} = 3$ kPa.

The h_{uu} capacity can be interpreted as follows:

- Since the mudline strength is negligible and this soil has been dragged down with the foundation, basal sliding resistance is assumed to be negligible.
- $h_{uu} = 3$ kPa can therefore be derived from a lateral pressure of $p_u \sim 8.5$ kPa acting on the front embedded area of the foundation ($w/D_f \sim 0.28$, $A_{front} = wD_f$ where w is embedment of the foundation). This value of p_u corresponds to approximately 2.8 times the average initial soil strength over the foundation embedded depth – i.e. a typical design value for this passive pressure ratio (Randolph and Gourvenec 2011).

4.2.1.2 Test 2: Consolidated-undrained capacity (h_{cu})

The consolidated-undrained resistance, h_{cu}, peaks at 15.5 kPa, far exceeding h_{uu} (by a factor of typically 5) at all displacements. The gain in capacity is due to consolidation of soil beneath the model foundation under the applied vertical preload during the initial consolidation period. Figure 13 presents the dissipation of excess pore pressure measured by the pore pressure transducer at the centre of the foundation invert. 80% of the excess pore pressure was dissipated during the initial consolidation, and the back-calculated coefficient of consolidation, c_v, is ~1.9 m^2/yr (interpreted against the numerical solution reported by Gourvenec and Randolph 2010). This is similar to the $c_v \sim 2.1$ m^2/yr from the initial consolidation of Test 3 (described later).

This consolidation-induced gain in the undrained shear strength underneath the foundation, $\Delta s_{u,c}$, can be estimated by an approach set out by Gourvenec et al. (2014) for shallow foundations. The increase in operative strength due to the preload can be estimated as

$$\Delta s_{u,c} = f_{su} f_{\sigma} \left(\frac{s_u}{\sigma'_{vo}} \right)_{NC} (V / A_{base}) \quad (3)$$

where f_{su} is a shear strength factor to account for the non-uniform distribution of the increase in shear strength and f_s is a stress factor to account for the non-uniform distribution of stress in the zone of soil affected by the preload (f_{su} f_s = 0.919 derived by Feng and Gourvenec (2015)); $(s_u/\sigma'_{v0})_{NC}$ is the normally-consolidated undrained shear strength ratio of the silt, which is ~0.5 based on laboratory tests (Chow et al. 2019). This approach would indicate a basal sliding component of 0.919 × 17 × 0.5 × 80% = 6.25 kPa, with the remaining 9.25 kPa of h_{cu} being due to the soil berm (w/D_f ~ 0.39, $A_{front} = wD_f$), i.e. p_u = 19 kPa. This soil berm component is approximately twice the resistance of the UU test at the same displacement, suggesting a doubling of the undrained strength of the soil berm following the disturbance during installation and the subsequent consolidation period.

4.2.1.3 Test 3: Cyclic consolidated undrained capacity ($h_{cyc,cu}$)

An even greater gain in capacity is evident in Table 6. The peak resistance after cycles of horizontal preloading and reconsolidation is $h_{cyc,cu}$ = 48.8 kPa which is ~3 times h_{cu}. Each one-way loading with reconsolidation represents an incremental cycle number of ΔN = 0.5, so initial installation is presented as N = 0, and the cyclic test starts from a cycle number of 0.5 for first horizontal loading to +75%h_{cu} and 1.0 during first loading reversal to -75%h_{cu}. The full response during the cyclic loading stage is shown in Figure 14a.

During each consolidation period, the soil underlying the foundation was subjected to the vertical preloading, v_{op} ~ 17kPa. The applied horizontal preloading, h_{op} ~ ±10 kPa would be shared between basal shear and passive resistance from the soil ahead of the foundation, consolidating this region.

The foundation settled by a further 0.06D_f (2.4 mm) during the cycles of horizontal loading. The amplitude of horizontal movement reduced from ±0.08D_f (3.2 mm) in the first cycle to only ±0.02D_f (0.8 mm) in the final cycle, reflecting a stiffening of the foundation soil (Figure 14b).

Each change in horizontal load created a pulse of positive excess pore pressure beneath the foundation. The pore pressure dissipation period was varied, allowing ~45% of excess pore pressure to dissipate after each change in load for the first 5 cycles, reducing to ~25% for the later cycles (Figure 14c). This pulse was smaller and dissipated more rapidly in later cycles,

reflecting densification of the foundation soil and a reduced tendency for generation of positive pore pressure. The changing apparent coefficient of consolidation, c_v, for each reconsolidation is back-calculated against the numerical solution reported by Gourvenec and Randolph (2010) (Figure 14d and e). The apparent c_v increases more rapidly over the first 5 cycles with T_{45} consolidation, and at a slightly lower rate for the rest of cycles with T_{25} consolidation. The final apparent c_v is 9 times higher than initial value (Figure 14f), which reflects that the soil underneath the foundation is compressed and the stiffness rises.

During the final loading stage to failure, a peak load of $h_{cyc,cu}$ = 48.8 kPa was recorded. This $h_{cyc,cu}$ capacity can be interpreted as follows:

- The initial consolidation and cyclic loading period (~200 mins, equivalent to T ~ 0.6, see Figure 13) is ~T_{95}, allowing 95% dissipation of the excess pore pressure generated by the vertical load, v_{op} ~ 17kPa. This consolidation-induced capacity can be estimated using Equation 3, and the basal sliding resistance is f_{su} f_s95%v_{op} $(s_u/\sigma'_{v0})_{NC}$ = 0.919 × 17 × 0.5 × 95% = 7.5 kPa.
- The remaining resistance (48.8 – 7.5 = 41.3 kPa) is from passive and active pressure on the front and rear of the foundation. It corresponds to a net lateral pressure of p_u ~69 kPa acting on the front and rear embedded areas of the foundation (w/D_f ~ 0.47, A_{front} = wD_f). This value of p_u is ~17 times the average initial soil strength over the embedded depth of the foundation (3.8 kPa from T-bar 2, so $p_u/s_{u,i}$ = 18), and is ~8 times greater than the value of p_u inferred from h_{uu} in test 1 (which was slightly shallower, as discussed earlier).
- The maximum lateral capacity factor on a circular foundation is $N_p = p_u/s_u$ = 12 (Martin and Randolph 2006). The calculated values of p_u imply that the soil strength in the active and passive zones has at least doubled during the cyclic loading phase relative to the initial value. At such shallow embedment a lower value of N_p applies, varying depending on the ratio of soil strength to unit weight. If a typical value of N_p = 6 is assumed, the soil strength increased by a factor of 3.

4.2.1.4 Summary of back-calculated changes in soil strength

The overall changes in foundation capacity between shallow foundation tests 1 to 3 are summarised in Table 6 as proportional increases relative to h_{uu}. These differences arise from changes in the basal sliding resistance and also the passive and active resistance on the

embedded area. The relative foundation capacity is not therefore directly proportional to changes in soil strength, but the following points summarise the interpretation described above:

- Consolidation under the foundation self-weight creates basal sliding resistance by raising the strength of the surface soil above the initial mudline value of zero. Together with an increase in the smaller passive resistance component, this consolidation causes h_{cu} to exceed h_{uu} by a factor of 5.
- The consolidation process during cycles of alternating horizontal load causes further strengthening of the surrounding soil. The elevated resistance is interpreted as fully consolidated undrained basal sliding coupled with at least a near-threefold rise in the strength of the passive and active soil zones, so that $h_{cyc,cu}$ exceeds h_{cu} by a factor of 3.

Ratios of the strength in the passive and active zones of 1:2:3 have been inferred from tests h_{uu}, h_{cu} and $h_{cyc,cu}$ respectively. For basal sliding, the mobilised strength assumed in $h_{cyc,cu}$ is 20% higher than in h_{cu}. Although the variation in soil strength from the sliding model foundation tests may not directly link to the strength interpreted from the penetrometer test, the foundation tests indicate a similar range in soil strength to that determined from the penetrometer test due to the combined effects of remoulding and reconsolidation.

4.2.2 Model foundation tests: buried plate foundation under vertical load

The results of the embedded plate tests are summarized in Table 6, and are presented in terms of the net penetration resistance, v, given by

$$v = v_m - \frac{F_b}{A_{base}} \tag{4}$$

where v_m is the measured penetration resistance, expressed as V_m/A_{base} in which V_m is the measured vertical force; F_b/A_{base} is the soil buoyancy term, in which F_b is the net upwards force due to the foundation (and its cylindrical shaft) becoming embedded in soil (rather than water) and is calculated as:

$$F_b = \begin{cases} \gamma' w A_{base}, & \text{if } w < t_{plate} \\ \gamma' \left[t_{plate} A_{base} + (w - t_{plate}) A_s \right], & \text{if } w \geq t_{plate} \end{cases} \tag{5}$$

where A_s represents the projected area of the cylindrical shaft; t_{plate} is the plate thickness; w is embedment depth of the plate; γ' is the effective unit weight of soil.

The resistance as the plate reached the depth of the sustained load test indicated the unconsolidated undrained capacity at that depth, in compression (v_{uu}) or tension ($v_{uu,tens}$). The

sustained load was ~75% of v_{uu} (test 4) and $v_{uu,tens}$ (test 6). The resistance in the subsequent test stage is the consolidated undrained foundation capacities, v_{cu} and $v_{cu,tens}$. In the cyclic compression test (test 5) and the cyclic tension test (test 7), the resistance in the subsequent test stage is the cyclic consolidated undrained foundation capacity, $v_{cyc,cu}$ and $v_{cyc,cu,tens}$.

The behaviour of the vertically-loaded plate is easier to interpret in terms of the changing soil strength compared to the horizontally-loaded surface foundation because the foundation capacity can be mapped more directly to soil strength (Zhou et al. 2019a; Zhou et al. 2019c Stanier and White 2019), since there are not separate components of basal sliding and passive/active resistance.

4.2.2.1 Test 4 and 5: Compression loading

The profiles of net penetration resistance for tests 4 and 5 are shown in Figure 15a. The resistance increases approximately linearly with depth, consistent with the strength profile. The resistance during extraction is lower than during penetration, because of the reduction in soil strength caused by partial remoulding.

Consolidation under sustained load leads to a 50% gain in capacity in compression (v_{cu} = 958 kPa for test 4), whereas the 10 cycles of episodic consolidation lead to a higher 70% gain in capacity ($v_{cyc,cu}$ = 1080 kPa for test 5) (Figure 15b, Table 6). During test 5, the settlement under ~75%v_{uu} progressively reduces with cycles, with a slow accumulation of embedment, as shown in Figure 15c and Figure 15d. This reflects the increase in stiffness and strength of the soil beneath the plate.

The changes in the soil stiffness are also evident in the pore pressure dissipation beneath the centre of the plate. The dissipation during each period of sustained load (at either ~10%v_{uu} or ~75%v_{uu}) is shown in Figure 16a. Each load was held for sufficient time for 90% dissipation of the excess pore pressure (T_{90}). The excess pore pressure has been normalised to unity after each change in load, and the time period has been made non-dimensional using a value of c_v that is selected to fit the numerical solution from Gourvenec and Randolph (2010). This fitting process allows a separate value of c_v to be identified for each dissipation stage, as shown in Figure 16b, and normalised to the initial value in Figure 16c. The apparent c_v in the first dissipation under the high sustained load (~75%v_{uu}) is used as the normalising value.

All unloading stages show an apparent c_v that is ~10 times this reference value, while during the loading phases the apparent c_v progressively rises by a factor of 10 over the first few cycles.

These observations indicate that the stiffening of the soil causes consolidation to occur approximately an order of magnitude faster than would be estimated using a c_v value appropriate to the initial stage.

Due to this shortening of the dissipation stages, the total duration of the episodic cyclic tests was therefore only approximately twice the 90% dissipation period from the first dissipation stage. This highlights that the high gains in strength evident in Table 6 can occur surprisingly rapidly, due to this quickening of the dissipation process.

4.2.2.2 Test 6 and 7: Tension loading

The profiles of net penetration resistance for tests 6 and 7 are shown in Figure 17a. The resistance during penetration and the initial extraction stage is comparable to tests 4 and 5, and the general effects of consolidation during tension loading match those seen for compression loading.

Consolidation under sustained load leads to a 15% gain in capacity in tension ($v_{cu,tens}$ = 375 kPa in test 6), whereas the 10 cycles of episodic consolidation lead to doubling of tension capacity ($v_{cyc,cu,tens}$ = 658 kPa in test 7) (Figure 17b). During test 7, the displacement when the maintained load of ~75%$v_{uu,tens}$ is applied progressively reduces with cycles (Figure 17c and Figure 17d). This reflects the increase in stiffness and strength of the soil above the plate.

The soil response beneath the plate is reflected in the pore pressure measured beneath the centre of the foundation. These results follow a similar pattern to the compression tests, although the rate of pore pressure dissipation is slower. The dissipation of excess pore pressure during each period of sustained load (at either ~10%$v_{uu,tens}$ or ~75%$v_{uu,tens}$) is shown in Figure 18a. Each load was held for consolidation periods between T_{50} and T_{90}.

Back analysis of the operative c_v follows the same manner used for the compression tests (tests 4 and 5). The resulting values of c_v for each dissipation stage are shown in Figure 18b, and normalised in Figure 18c by the apparent c_v in the initial dissipation under the high sustained load (~75%$v_{uu,tens}$). The initial value of c_v ~50 m^2/year is an order of magnitude higher than during the subsequent consolidation periods. A minimum value of c_v = 2 m^2/year is obtained from the consolidation at N = 0.5. After that, the apparent c_v inferred from dissipation under 10%$v_{uu,tens}$ gradually increased to ~15 m^2/year and under 75%v$_{uu,tens}$ to ~10 m^2/year. The generally low values could reflect that the dissipation process involves seepage flow of water into a gap that may have been opening beneath the plate, so would take longer than if the

drainage was solely within the soil. Han et al. (2016) reported results from a set of particle image velocimetry tests on a strip anchor in clay under sustained tensile load and consolidation that demonstrate a similar phenomenon. Their data showed that during consolidation with intermediate levels of the uplift load (i.e. 60-80% of the $v_{uu\text{-}tens}$) seepage of pore pressure from the surrounding soil results in separation between the anchor base and the soil, and then a gap at the base of the anchor is developed. The progressive increase in apparent c_v could be associated with stiffening of the soil, in the same manner as seen for the compression tests.

4.2.2.3 Summary of back-calculated changes in soil strength

The buried plate tests show that the trends of changing strength evident in the penetrometer tests (Section 3) are mirrored in the foundation capacity of a deeply buried foundation, subjected to either compression or tension loading. Under sustained load, allowing time for almost full pore pressure dissipation, the foundation capacity rises by 50% on average. After 10 cycles of loading with almost full pore pressure dissipation at each load level, the gain is on average 90%.

During the episodic consolidation phases, each change in load creates a step change in excess pore pressure. The dissipation of this pore pressure quickens progressively through the cycles such that the high gains in strength evident in Table 6 occur surprisingly rapidly.

5. CONCLUSIONS

This paper has illustrated the strong influences of remoulding and reconsolidation on foundation capacity and penetrometer resistance, through a program of centrifuge modelling.

The penetrometer tests were performed using model scale T-bar and piezoball penetrometers that were penetrated either statically or cyclically. The initial variation with depth of soil strength was affected by inadvertent steady downward seepage through the sample. However, this has no effect on the relative changes in penetration and extraction resistances and therefore soil strength at a given depth.

The results demonstrate that undrained strength can vary by a factor of 15 between a fully remoulded state (after cyclic loading) and a long term limiting state (after episodes of remoulding and reconsolidation). Previous studies have assessed these effects in kaolin clay and this study extends the observation to a natural reconstituted carbonate silt.

For the model foundation tests, the soil strength back-calculated from the foundation capacity of a surface or embedded foundation can be increased by 50% on average considering effects

of consolidation and sustained load, and the long-term episodes of loading and consolidation can enhance the effect and lead to three times higher than the initial (undrained-unconsolidated) value.

Together, these observations and the associated back-calculation methods, offer the possibility of unlocking better utilisation of 'whole life' foundation capacity by quantifying the expected gains in strength through novel penetrometer tests. Consideration needs to be given to the spatial and temporal extents of these soil strength increases, to support their inclusion in design scenarios. More confidence will grow as additional testing of this kind in different soils is performed, to examine how the magnitude of the changes in strength vary with soil type, including in intact deposits.

6. ACKNOWLEDGEMENTS

The first author acknowledges his research studentship support from the ARC Industrial Transformation Research Hub for Offshore Floating Facilities and the University of Western Australia. This work forms part of the activities of the Centre for Offshore Foundation Systems (COFS), currently supported as a node of the Australian Research Council's Centre of Excellence for Geotechnical Science and Engineering, and through the Fugro Chair in Geotechnics, the Lloyd's Register Foundation Chair and the Shell Chair in Offshore Engineering.

7. NOTATION

A_{base}	projected area of the model foundation
A_{front}	frontal embedded area of the model foundation
c_v	coefficient of vertical consolidation
c_h	coefficient of horizontal consolidation
D_{PB}	piezoball diameter
$D_{shaft,PB}$	piezoball shaft diameter
$D_{T\text{-}bar}$	T-bar diameter
$D_{shaft,T\text{-}bar}$	T-bar shaft diameter
D_f	foundation diameter
$D_{shaft,f}$	diameter of model foundation shaft
F_b	buoyancy force
G_s	specific gravity
g	earth's gravitational acceleration, 9.81 m/s^2
h	foundation capacity for the horizontally-loaded plate
h_{uu}	undrained unconsolidated horizontal capacity
h_{cu}	consolidated undrained horizontal capacity
$h_{cyc,cu}$	cyclic consolidated undrained horizontal capacity
H	horizontal load
k_i	strength gradient during initial penetration
k_{cyc}	strength gradient during cyclic penetration
k	strength gradient
$\triangle k$	strength gradient ratio
LL	liquid limit

N_p	lateral capacity factor
$N_{T\text{-}bar}$	capacity factor for T-bar penetrometer
N_{ball}	capacity factor for ball penetrometer
N	cycle number
PL	plastic limit
q_{PB}	piezoball penetration resistance
s_u	undrained shear strength
$(s_u/\sigma'_{v0})_{NC}$	normally consolidated strength ratio
t	time
t_f	thickness of model foundation
T	dimensionless time
u	horizontal displacement
u_e	excess pore pressure
$u_{e,i}$	initial excess pore pressure
V	vertical force
v	foundation capacity for the embedded plate
v_{op}	vertical loading pressure
v_{uu}	undrained unconsolidated vertical capacity
v_{cu}	consolidated undrained vertical capacity
$v_{cyc,cu}$	cyclic consolidated undrained vertical capacity
$v_{cu,tens}$	consolidated undrained vertical tensile capacity
$v_{cyc,cu,tens}$	cyclic consolidated undrained vertical tensile capacity
w	foundation embedment
z	depth

M, Γ, λ, κ	critical state parameters
σ_{vo}	vertical overburden stress
σ'_v	vertical effective stress
γ'	soil effective unit weight

8. REFERENCES

Andersen, K.H., Kleven, A., and Heien, D. 1988. Cyclic soil data for design of gravity structures. *Journal of Geotechnical Engineering, ASCE*, 114, 5, 517–539.

Andersen, K.H. 2015. Cyclic soil parameters for offshore foundation design. In *Frontiers in Offshore Geotechnics–ISFOG* III. 3-82, Oslo, Norway, Taylor and Francis Group, London.

API 2005. *API recommended practice - 2SK Design and Analysis of Stationkeeping Systems for Floating Structures*. American petroleum institute.

Amodio, A., Chang, T.M., Kong, V., and Erbrich, C. 2015. The effects of jack-up installation procedures on spudcan capacity in offshore carbonate sediments. In *Frontiers in Offshore Geotechnics –ISFOG III* (Ed. Meyer, V.), 1253-1260. Oslo, Norway: CRC Press.

Bienen, B., and Cassidy, M.J. 2013. Set-up and resulting punch through risk of jack-up spudcans during installation. *J. Geotech. Geoenviron. Engng*, ASCE 139, No. 12, 2048–2059.

Bransby, M.F. 2002. The undrained inclined load capacity of shallow foundations after consolidation under vertical loads. In *Numerical models in geomechanics* – NUMOG VIII (eds G. N. Pande and S. Pietruszczak), pp. 431–437. Boca Raton, FL, USA: CRC Press.

Chow, S.H., O'Loughlin, C.D., Zhou, Z., White, D.J., and Randolph, M.F. 2019. Penetrometer testing in a calcareous silt to explore changes in soil strength. *Géotechnique*. Ahead of print online, doi.org/10.1680/jgeot.19.P.069.

Chung, S.F., and Randolph, M.F. 2004. Penetration resistance in soft clay for different shaped penetrometers. *Proc., of 2ed Int. Conf. on Site Characterisation*. Porto, Portugal, Vol. 1, Millpress, Rotterdam: 671-677.

Cocjin, M.L., Gourvenec, S.M., White, D.J., and Randolph, M.F. 2014. Tolerably mobile subsea foundations-observations of performance. *Géotechnique*, 64(11), 895-909.

Cocjin, M.L., Gourvenec, S.M., and White, D.J. 2017. Softening and consolidation around seabed pipelines: centrifuge modelling. *Géotechnique*, 68(2), 118-132.

DeJong, J.T., and Randolph, M.F. 2012. Influence of partial consolidation during cone penetration on estimated soil behavior type and pore pressure dissipation measurements.

Journal of Geotechnical and Geoenvironmental Engineering, 138(7), 777–788.

Dejong, J., Yafrate, N., DeGroot, D., Low, H.E., and Randolph, M.F. 2010. Recommended practice for full flow penetrometer testing and analysis, *ASTM Geotechnical Journal*, 33(2), p GJT102468.

DNV GL 2018a. *DNV GL – RP – E301 Design and installation of fluke anchors in clay*. DNV GL AS.

DNV GL 2018b. *DNV GL – RP – E302 Design and installation of plate anchors in clay*. DNV GL AS.

Einav, I., and Randolph, M.F. 2005. Combining upper bound and strain path methods for evaluating penetration resistance. *International Journal for Numerical Methods in Engineering* **63**, No. 14, 1991-2016.

Feng, X., and Gourvenec, S. 2015. Consolidated undrained load carrying capacities of mudmats under combined loading in six degrees-of-freedom. *Géotechnique*, 65(7), 563–575.

Fu, D., Gaudin, C., Tian, C., Bienen, B., and Cassidy, M.J. 2015. Effects of preloading with consolidation on undrained bearing capacity of skirted circular footings. *Géotechnique* 65(3), 231–246.

Gaudin, C., White, D.J., Boylan, N., Breen, J., Brown, T.A., De Catania, S., and Hortin, P. 2009. A wireless data acquisition system for centrifuge model testing. *Measurement Science and Technology*, Vol. 20, No 095709.

Gourvenec, S., and Randolph, M.F. 2010. Consolidation beneath circular skirted foundations, *International Journal for Geomechanics*, 10(1), 22-29.

Gourvenec, S., Vulpe, C., and Murphy, T.G. 2014. A method for predicting the consolidated undrained bearing capacity of shallow foundations. *Géotechnique*, 64(3), 215–225.

Gourvenec, S.G., Feng, X., Randolph, M.F., and White, D.J. 2017. A toolbox of technologies to optimise subsea foundation design. *Proceedings of the offshore technology conference*, Houston, TX, USA, paper OTC 27703.

Hodder, M.S., White, D.J., and Cassidy, M.J. 2013. An effective stress framework for the variation in penetration resistance due to episodes of remoulding and reconsolidation. *Géotechnique*, 63(1), 30-43.

House, A., Olivera, J.R.M.S., and Randolph, M.F. 2001. Evaluating the coefficient of consolidation using penetration tests. *International Journal of Physical Modelling in Geotechnics*, 3, 17 – 25.

Hossain, M.S., and Randolph, F.M. 2009. New mechanism-based design approach for spudcan foundations on single layer clay. *Journal of Geotechnical and Geoenvironmental Engineering*. 135(9), 1264-1274.

Hossain, M.S., Hu, Y., Randolph, F.M., and White, J.D. 2005. Limiting cavity depth for spudcan foundations penetrating clay. *Géotechnique*. 55(9), 679-690.

ISO 2013. *ISO 19901-7 Petroleum and natural gas industries – Specific requirements for offshore structures – part 7*. International standard.

ISO 2014. *ISO 19901-3 Petroleum and natural gas industries – Specific requirements for offshore structures – part 3*. International standard.

Low, H.E., Lunne, T., Andersen, H.K., Sjursen, A.M., Li, X., and Randolph, F.M. 2010. Estimation of intact and remoulded undrained shear strengths from penetration tests in soft clays. *Géotechnique*, 60(11), 843-859.

Low, H.E. 2009. Performance of penetrometers in deep-water soft soil characterisation. PhD thesis, The University of Western Australia, Perth, Australia.

Lehane, B.M., and Jardine, R.J. 2003. The effect of long term preloading on the performance of a vertically loaded footing on Bothkennar clay. Géotechnique 53(8), 689–695.

Lehane, B.M., and Gaudin, C. 2005. Effects of drained preloading on the performance of shallow foundations on overconsolidated clay. Proceedings of the 24th international conference of offshore mechanics and arctic engineering, Halkidiki, Greece, vol. 2, pp. 891–896. New York, NY, USA: American Society of Mechanical Engineers.

Li, X., Gaudin, C., Tian, Y., and Cassidy, M.J. 2015. Effects of preloading and consolidation on the uplift capacity of skirted foundations. *Géotechnique*, 65(12), 1010–1022.

Mahmoodzadeh, H., Wang, D., and Randolph, M.F. 2015. Interpretation of piezoball dissipation testing in clay. *Géotechnique*, 65(10), pp.831–842.

Martin, C.M., and Randolph, M.F. 2006. Upper-bound analysis of lateral pile capacity in cohesive soil. *Géotechnique*, 52(6), 141-145.

O'Loughlin, C.D., Zhou, Z., Stanier, S.A., and White, D.J. 2019. Load-controlled cyclic T-bar tests: A new method to assess the combined effects of cyclic loading and consolidation. *Géotechnique letters*, 10(1), 1-9.

Purwana, O.A., Leung, C.F., Chow, Y.K., and Foo, K.S. 2005. Influence of base suction on extraction of jack-up spudcans. *Géotechnique* **55(**10), 741–753.

Randolph, M.F. and Hope, S. 2004. Effect of cone velocity on cone resistance and excess pore pressures. In *Proceedings of the International Symposium on Deformation Characteristics of Geomaterials – IS Osaka*. The Hague, The Netherlands, pp. 147–152.

Randolph, M.F., and Gourvenec, S.M. 2011. Offshore Geotechnical Engineering. Spon Press

Randolph, M.F., Jewell, R.J., Stone, K.J.L., and Brown, T.A. 1991. Establishing a new centrifuge facility. *Proceedings of international conference on centrifuge modelling, Centrifuge 91*. Boulder, Colorado, 3-9.

Ragni, R., Wang, D., Mašín, D., Bienen, B., Cassidy, M., and Stanier, S. 2016. Numerical modelling of the effects of consolidation on jack-up spudcan penetration. *Computers and Geotechnics*, Volume 78, 25-37.

Stanier, S.A., and White, D.J. 2019. Enhancement of bearing capacity from consolidation: due to changing strength or failure mechanism? *Géotechnique*, 69(2), 166-173

Stewart, D.P., and Randolph, M.F. 1991. A new site investigation tool for the centrifuge. In *Proceedings of international conference on centrifuge modelling, Centrifuge 91*. Boulder (eds.-Y. Ko and F. G. McLean), 531–538. Rotterdam, the Netherlands: Balkema.

Stewart, D.P., and Randolph, M.F. 1994. T-Bar penetration testing in soft clay. *Journal of Geotechnical Engineering*, ASCE, 120, 12, pp. 2230-2235.

Teh, C.I., and Houlsby, G.T. 1991. An analytical study of the cone penetration test in clay. *Geotechnique*, 41(1), pp.17–34.

White, D.J., Gaudin, C., Boylan, N., and Zhou, H. 2010. Interpretation of T-bar penetrometer tests at shallow embedment and in very soft soils. *Canadian Geotechnical Journal*, 47(2):218-229

Wang, D., and Bienen, B. 2016. Numerical investigation of penetration of a large-diameter footing into normally consolidated kaolin clay with a consolidation phase. *Géotechnique*,

66(11), 947-952.

Zdravkovic, L., Potts, D.M., and Jackson, C. 2003. A numerical study of the effect of pre-loading on undrained bearing capacity. *Int. J. Geomech*. 3, No. 1, 1–10.

Zhou, Z., White, D.J., and O'Loughlin, C.D. 2019a. An effective stress framework for estimating penetration resistance accounting for changes in soil strength from maintained load, remoulding and reconsolidation. *Géotechnique,* **69**(1), 57-71.

Zhou, Z., O'Loughlin, C.D., White, D.J., and Stanier, S.A. 2019b. Improvements in plate anchor capacity due to cyclic and maintained loads combined with consolidation. *Géotechnique.* Ahead of print, doi.org/10.1680/jgeot.19.ti.028.

Zhou, Z., O'Loughlin, C.D., and White, D.J. 2019c. An effective stress analysis for predicting the evolution of SCR–seabed stiffness accounting for consolidation. *Géotechnique.* Ahead of print, doi: 10.1680/jgeot.18.P.313.

Zhou, H. and Randolph, F.M. 2009. Numerical investigations into cycling of full-flow penetrometers in soft clay. *Géotechnique,* **59**(10), 801-812.

9. FIGURE CAPTIONS

Figure 1 Apparatus: (a) model foundation; (b) T-bar and piezoball

Figure 2 (a) Experimental arrangement for the foundation tests; (b) Experimental arrangement for the penetrometer tests; (c) Test plan

Figure 3 (a) Undrained shear strength profiles from cyclic T-bar tests; (b) soil strength variation ratio, $s_{u,cyc}/s_{u,i}$, at $z/D_{T\text{-}bar} = 33$

Figure 4 Variation of coefficient of consolidation with vertical effective stress, σ'_v (data from Chow et al. 2019)

Figure 5 Time history of penetration depth during: (a) episodic T-bar test; (b) episodic cyclic piezoball test

Figure 6 Evolution of undrained shear strength profile with cycle number in the episodic T-bar test

Figure 7 (a) Development of trench depth against number of cycles from this study and the test reported by Cocjin et. al (2014); (b) trench observed in footprint after test completion

Figure 8 Strength changes during the episodic cyclic T-bar test and an equivalent test in kaolin clay reported by Cocjin et. al (2014)

Figure 9 Initial dissipation of excess pore pressure (before cyclic phase) at depths, $z/D_{PB} = 4$ and 10.5

Figure 10 Results of the episodic cyclic piezoball tests: (a) profile of soil strength for the first phase; (b) cyclic evolution of normalised soil strength at $z/D_{PB} = 4$; (c) profile of soil strength for the second phase; (d) cyclic evolution of normalised soil strength at $z/D_{PB} = 10.5$

Figure 11 Time histories (at model scale) of (a) operative vertical loading, v_{op}, and overview of test procedures for surface model foundation tests (Test 1, 2 and 3); (b) operative horizontal loading, h_{op}, applied in Test 3; (c) operative vertical loading in embedded plate tests (Test 4 to 7)

Figure 12 Responses during loading to failure (surface foundation tests): (a) horizontal resistance against normalised horizontal displacement, u/D_f; (b) trajectory

Figure 13 Dissipation response during initial consolidation (tests 2 and 3)

Figure 14 Shallow foundation (test 3): (a) horizontal load history; (b) settlement and horizontal displacement; (c) pore water pressure at foundation base throughout cyclic loading phases; (d) normalised excess pore pressure against time; (e) normalised excess pore pressure against dimensionless time; (f) apparent variation in coefficient of consolidation with cycles of consolidation

Figure 15 Buried plate compression tests (Test 4 and 5): (a) overall penetration resistance profiles; (b) sustained and cyclic loading phases; (c) consolidation settlement under sustained load ($75\%v_{uu}$); (d) increase in normalised embedment through cycles under $75\%v_{uu}$

Figure 16 Buried plate test 5: (a) normalised excess pore pressure dissipation; (b) variation in apparent consolidation coefficient, c_v; (c) proportional rise in an apparent consolidation coefficient, $c_v/c_{v,i}$

Figure 17 Buried plate tension tests (Test 6 and 7): (a) overall penetration resistance profiles; (b) sustained and cyclic loading phases; (c) consolidation settlement under sustained load (75%$v_{uu,tens}$); (d) reduction normalised in embedment through cycles under 75%$v_{uu,tens}$

Figure 18 Buried plate test 5: (a) normalised excess pore pressure dissipation; (b) variation in apparent consolidation coefficient, c_v; (c) proportional rise in an apparent consolidation coefficient, $c_v/c_{v,i}$

10. TABLE CAPTIONS

Table 1 Geometric details of model foundation and penetrometers

Table 2 Characteristics of the natural carbonate silt (Chow et al. 2019)

Table 3 Centrifuge test programme

Table 4 Procedures in horizontally-loaded shallow foundation tests

Table 5 Procedures in vertically-loaded plate foundation tests

Table 6 Observed changes in foundation capacity from cyclic loading and consolidation

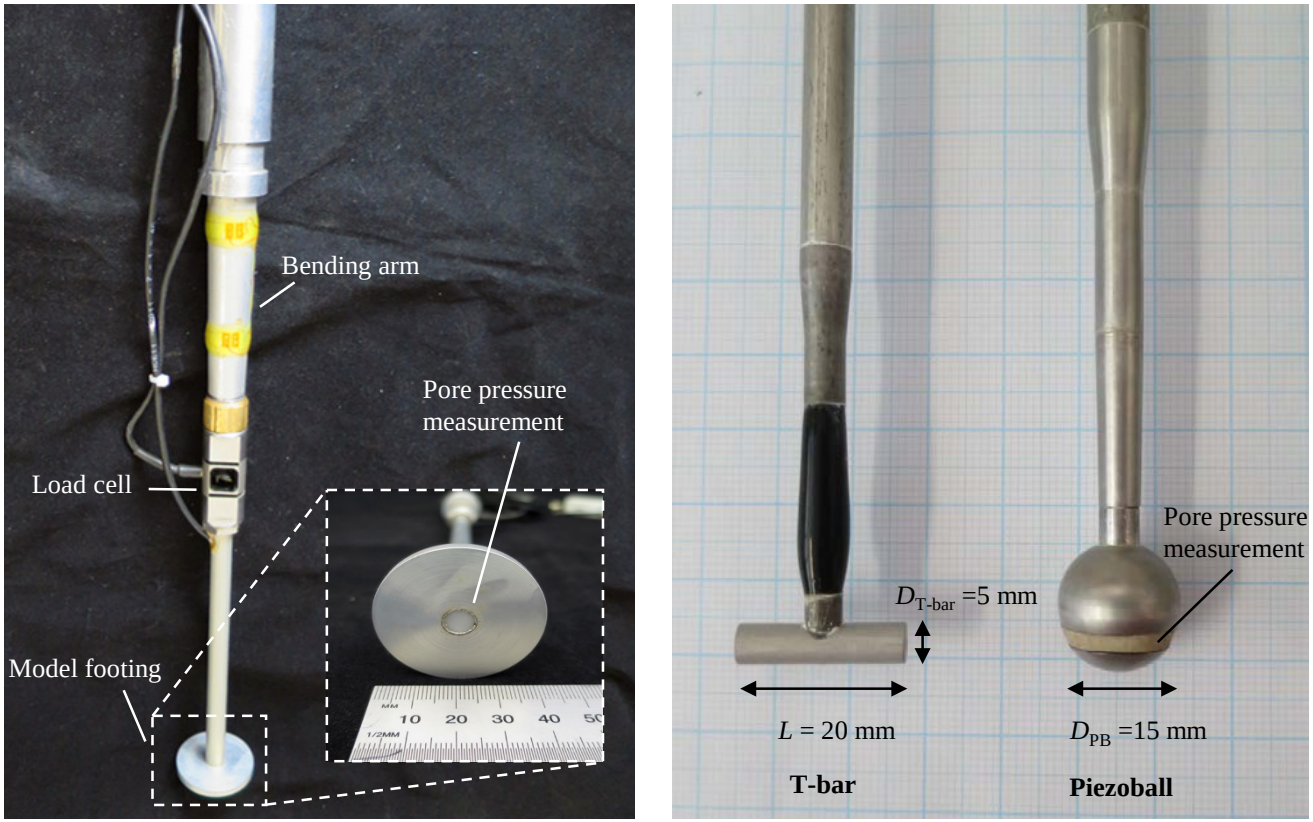

(a) (b)

Figure 1 Apparatus: (a) model foundation; (b) T-bar and piezoball

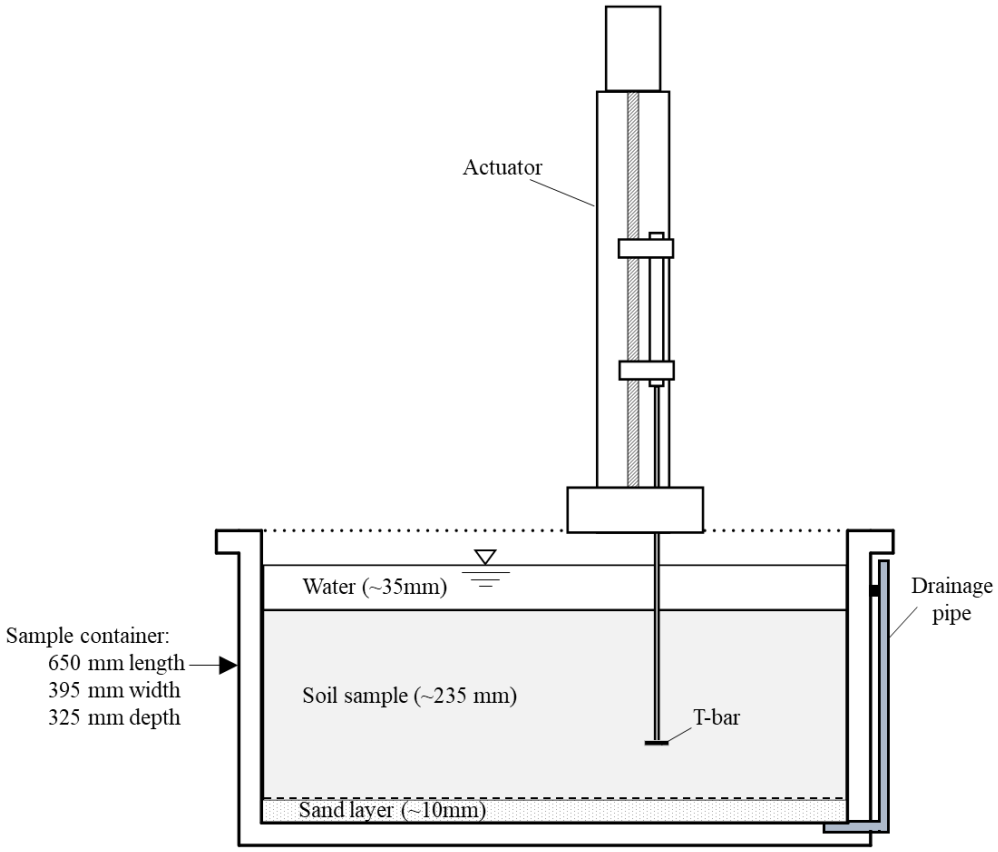

(a)

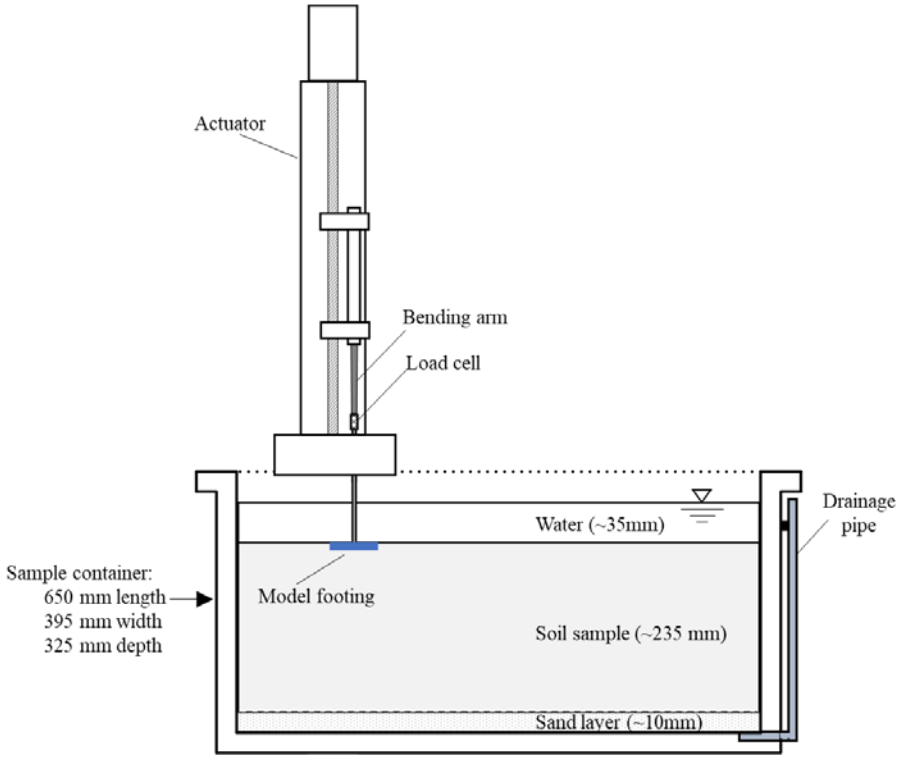

(b)

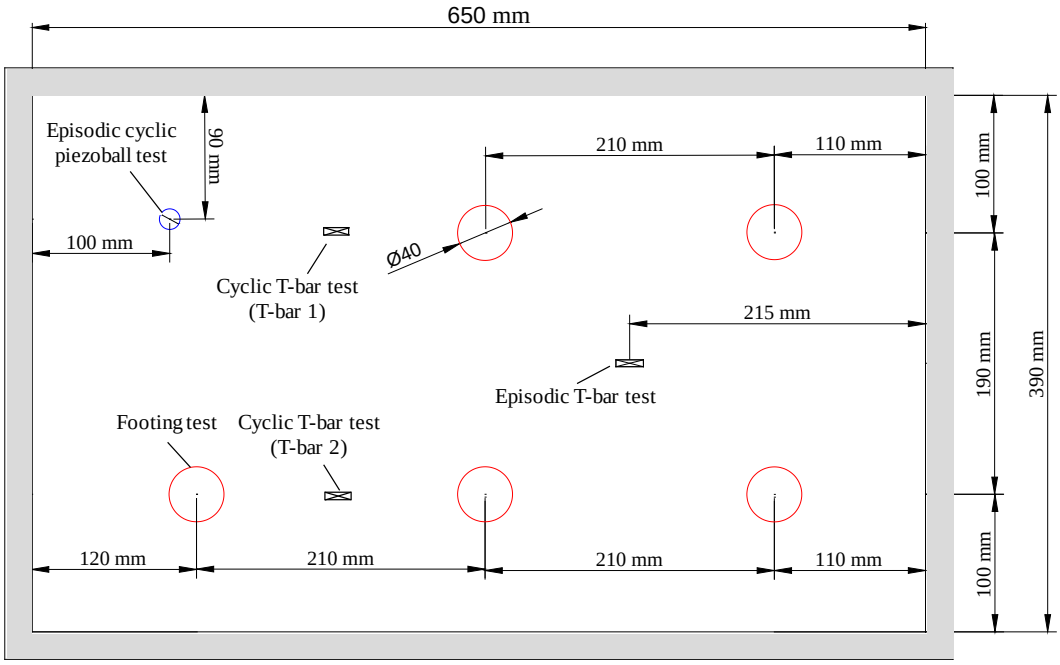

(c)

Figure 2 (a) Experimental arrangement for the foundation tests; (b) Experimental arrangement for the penetrometer tests; (c) Test plan

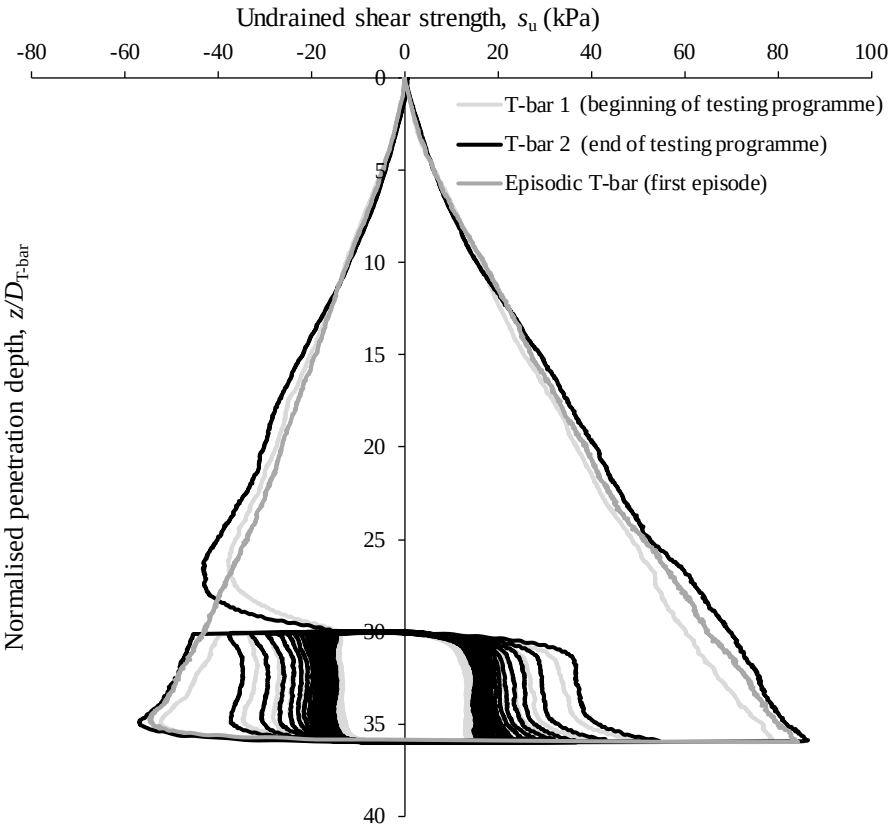

(a)

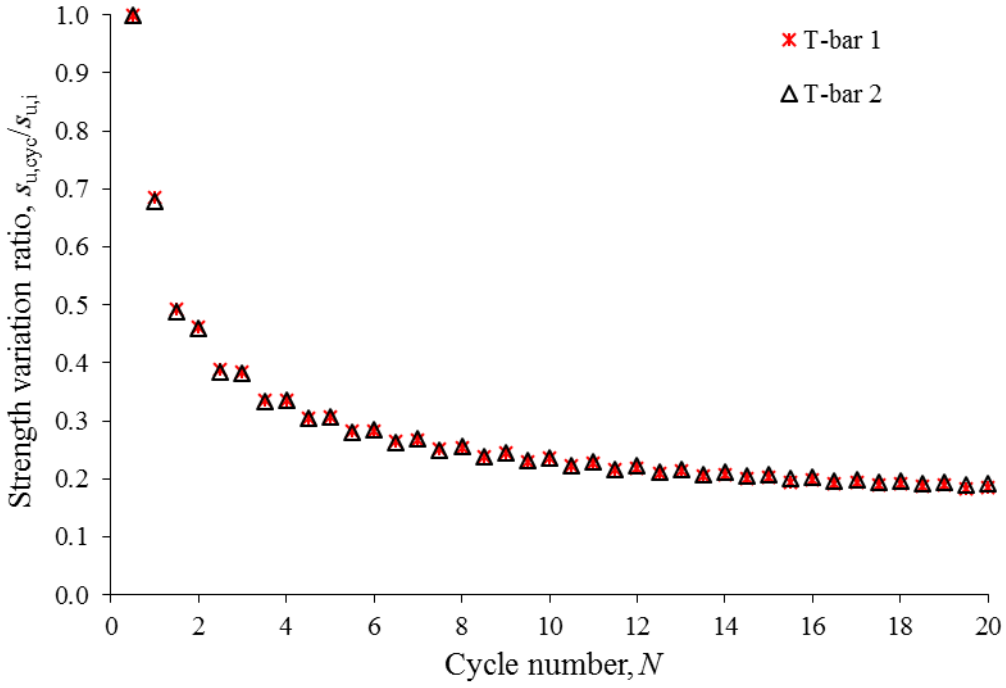

(b)

Figure 3 (a) Undrained shear strength profiles from cyclic T-bar tests; (b) soil strength variation ratio, $s_{u,cyc}/s_{u,i}$, at $z/D_{T\text{-}bar}$ = 33

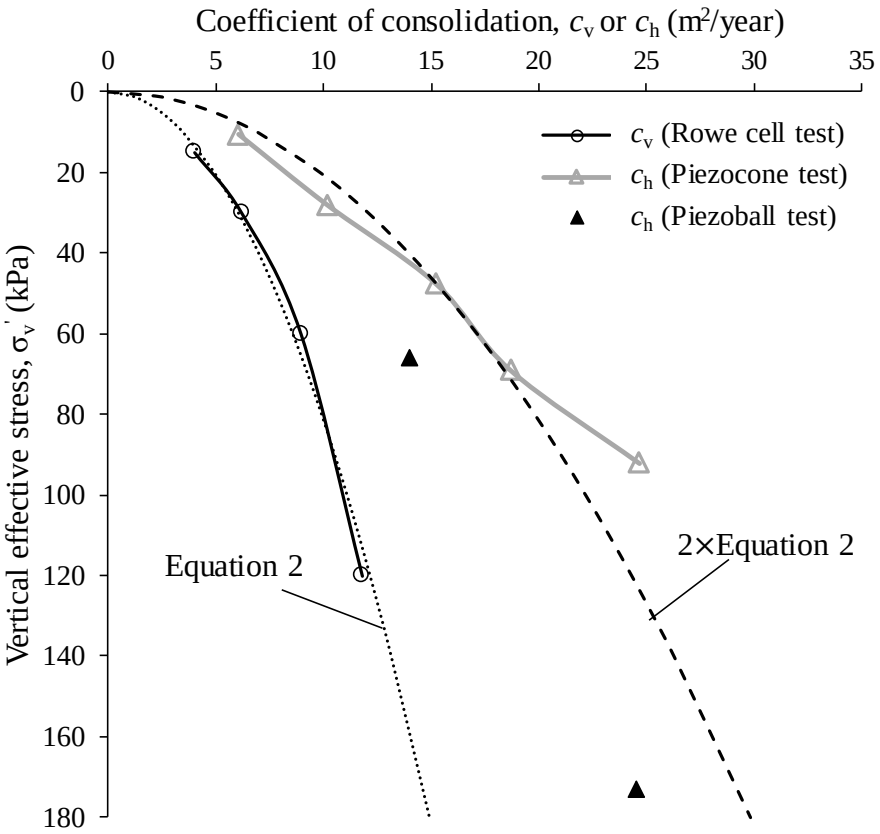

Figure 4 Variation of coefficient of consolidation with vertical effective stress, σ'_v *(data from Chow et al. 2019)*

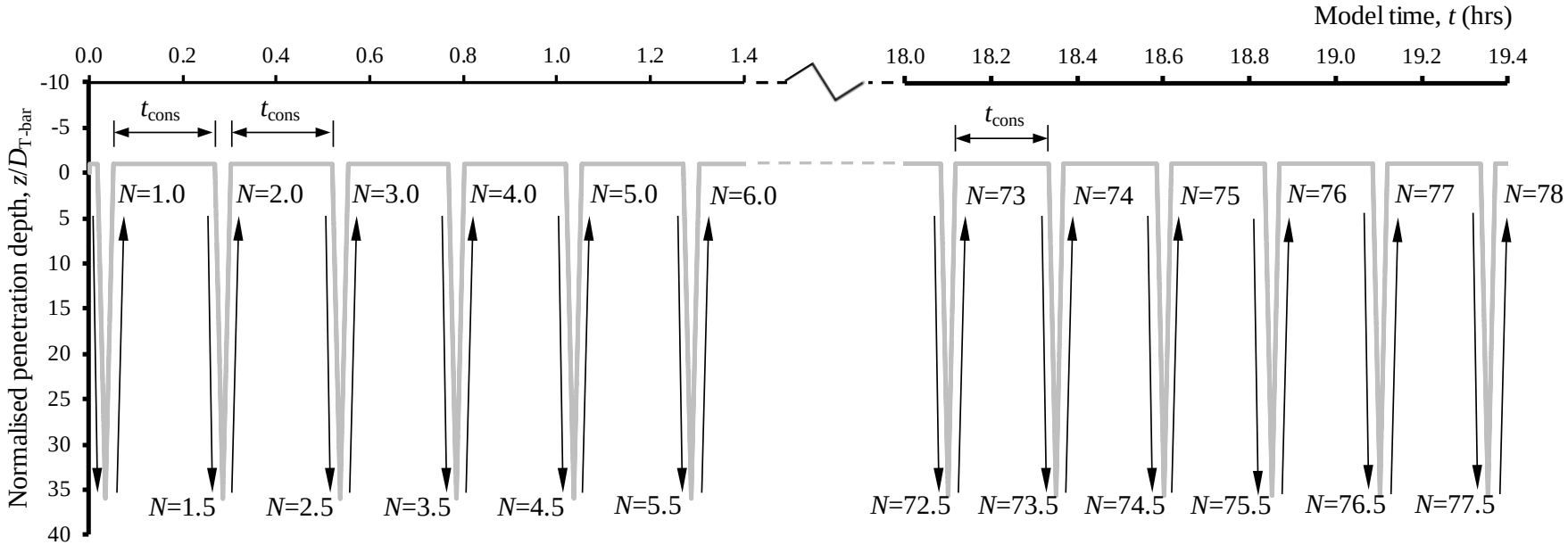

(a)

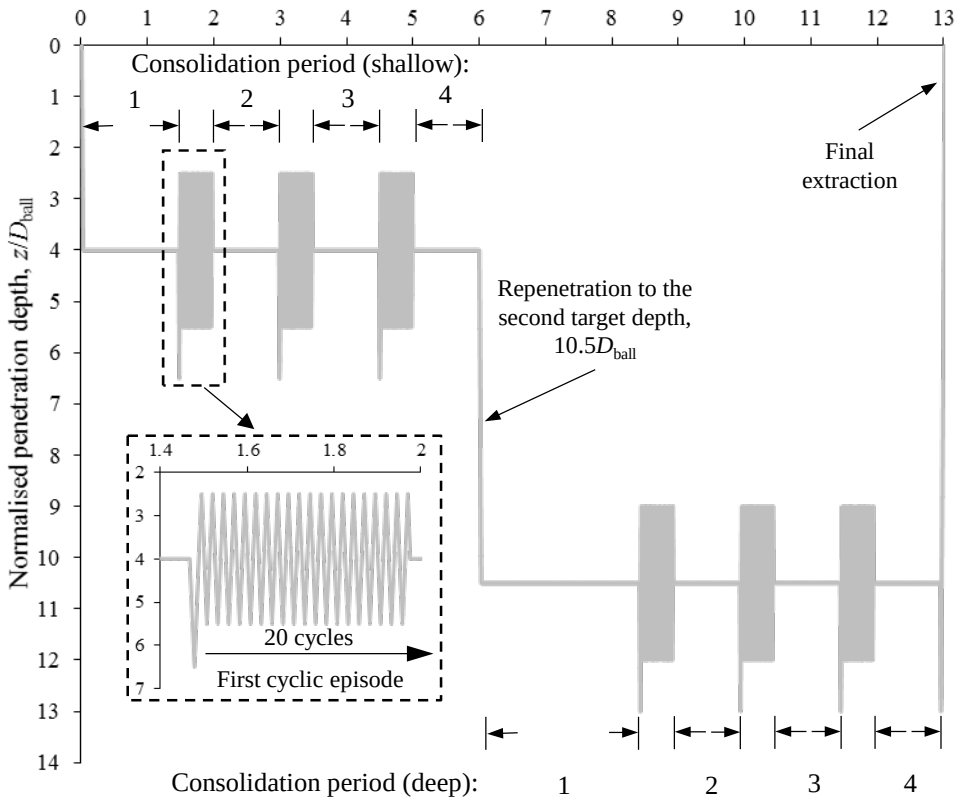

(b)

Figure 5 Time history of penetration depth during: (a) episodic T-bar test; (b) episodic cyclic piezoball test

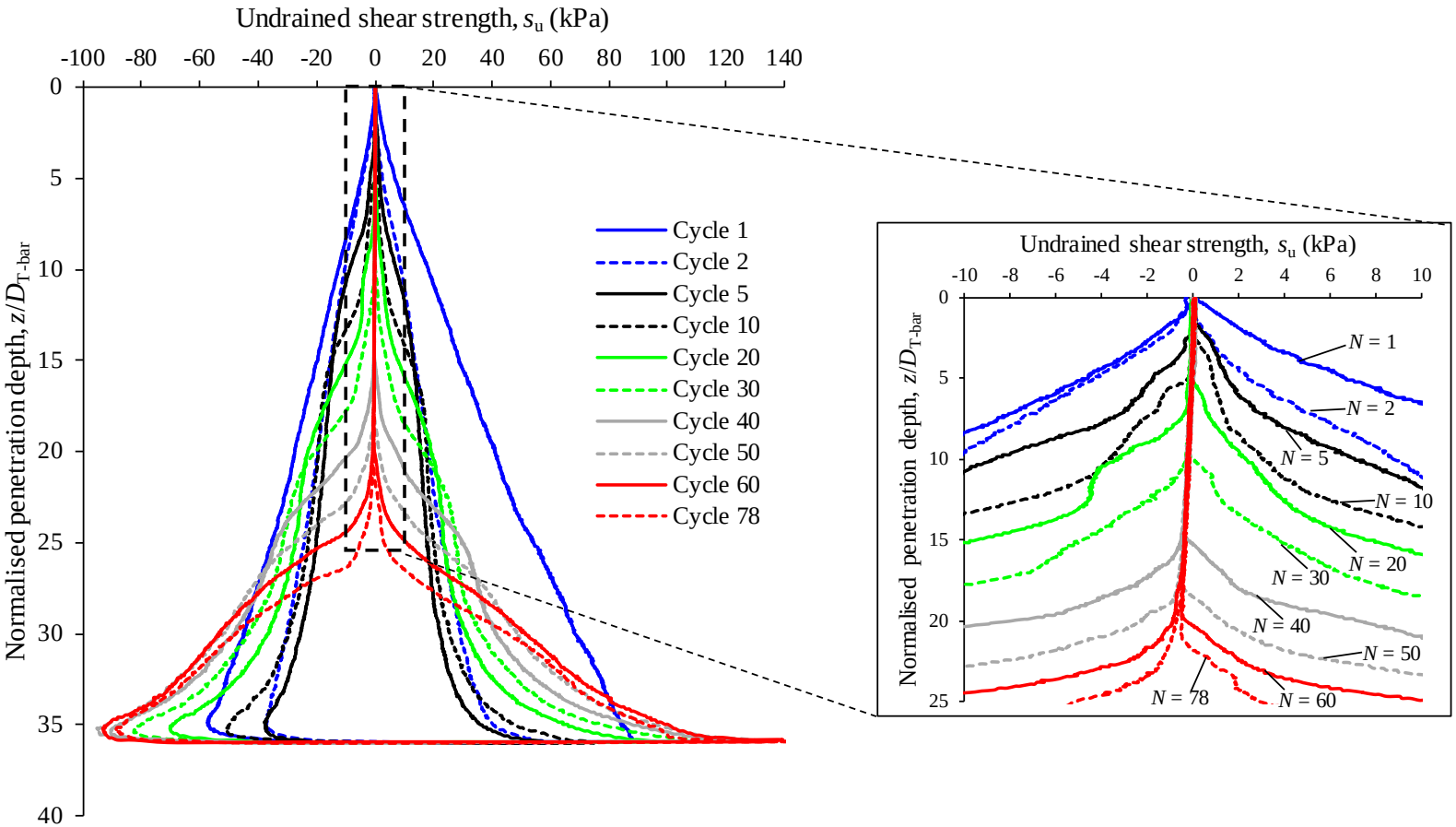

Figure 6 Evolution of undrained shear strength profile with cycle number in the episodic T-bar test

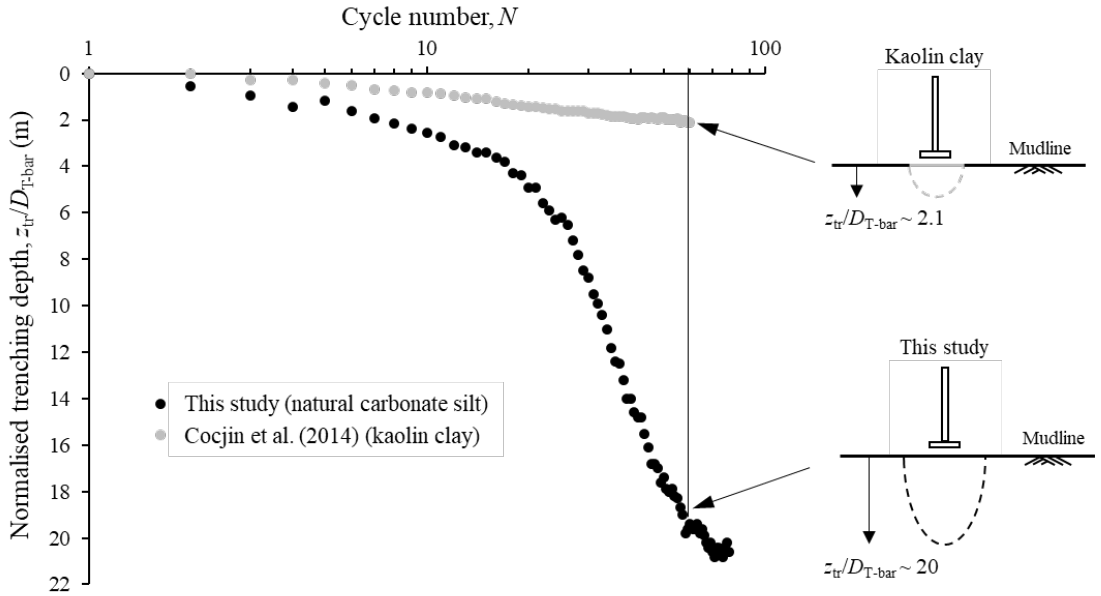

(a)

(b)

Figure 7 (a) Development of trench depth against number of cycles from this study and the test reported by Cocjin et. al (2014); (b) trench observed in footprint after test completion

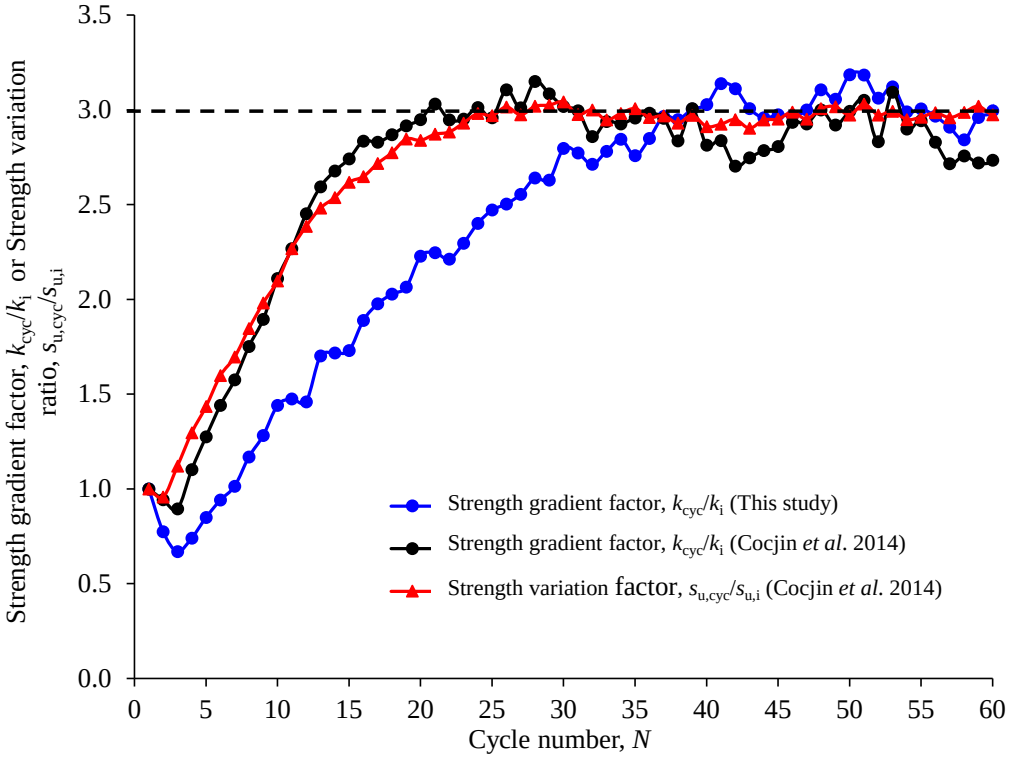

Figure 8 Strength changes during the episodic cyclic T-bar test and an equivalent test in kaolin clay reported by Cocjin et. al (2014)

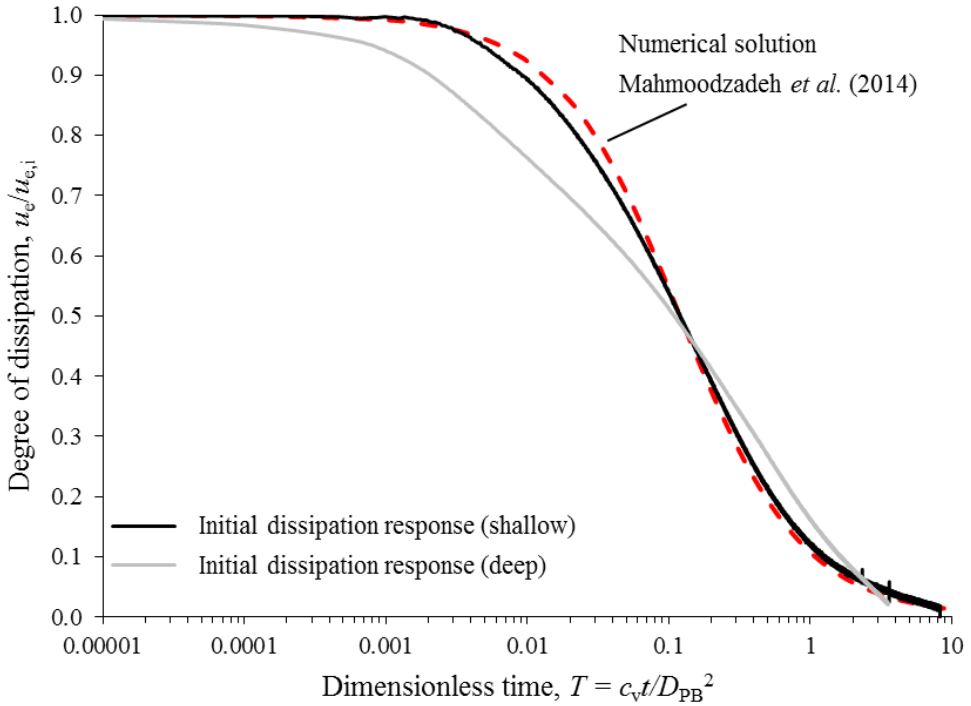

Figure 9 Initial dissipation of excess pore pressure (before cyclic phase) at depths, z/D_{PB} = 4 and 10.5

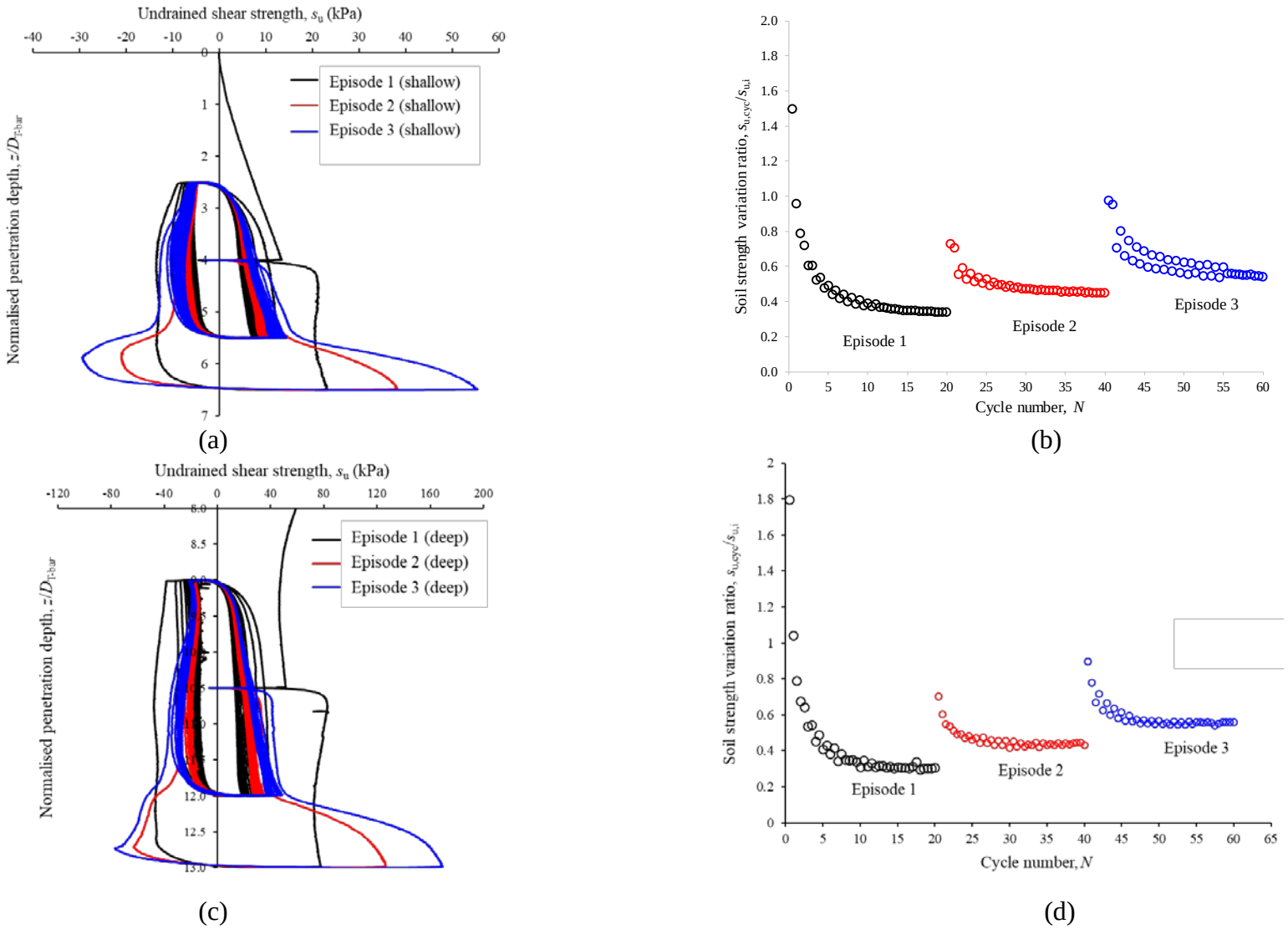

Figure 10 Results of the episodic cyclic piezoball tests: (a) profile of soil strength for the first phase; (b) cyclic evolution of normalised soil strength at z/D_{PB} = 4; (c) profile of soil strength for the second phase; (d) cyclic evolution of normalised soil strength at z/D_{PB} = 10.5

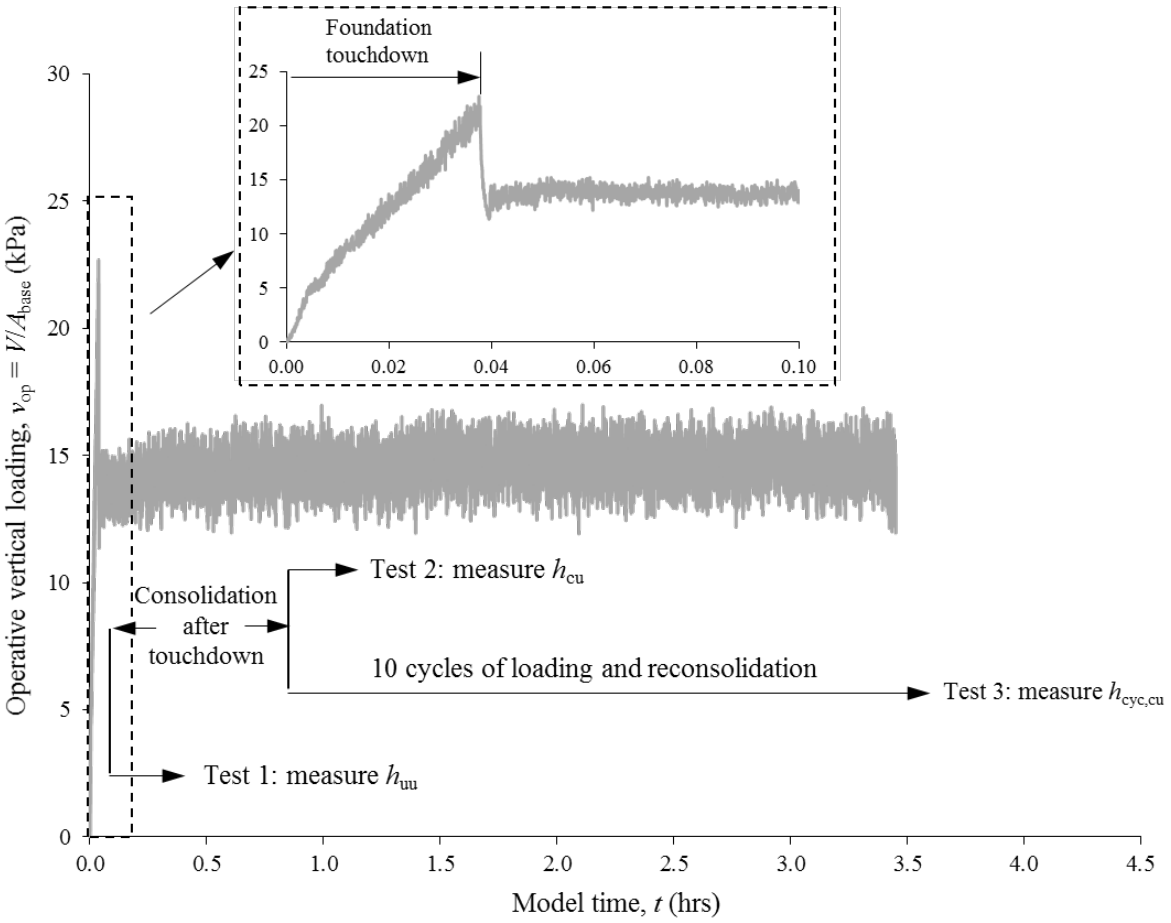

(a)

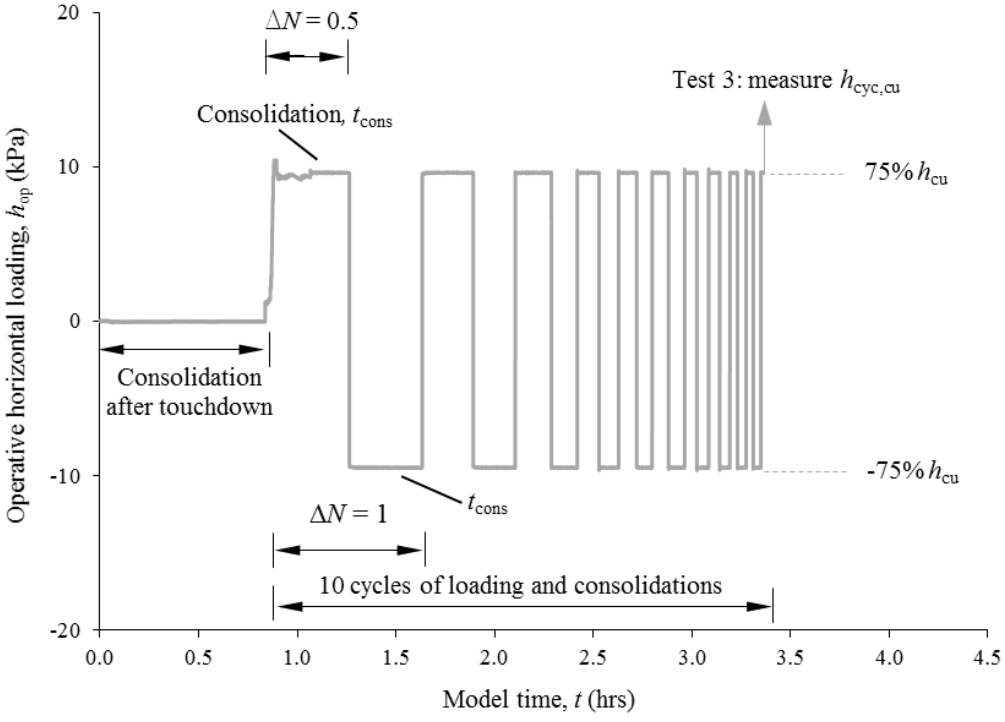

(b)

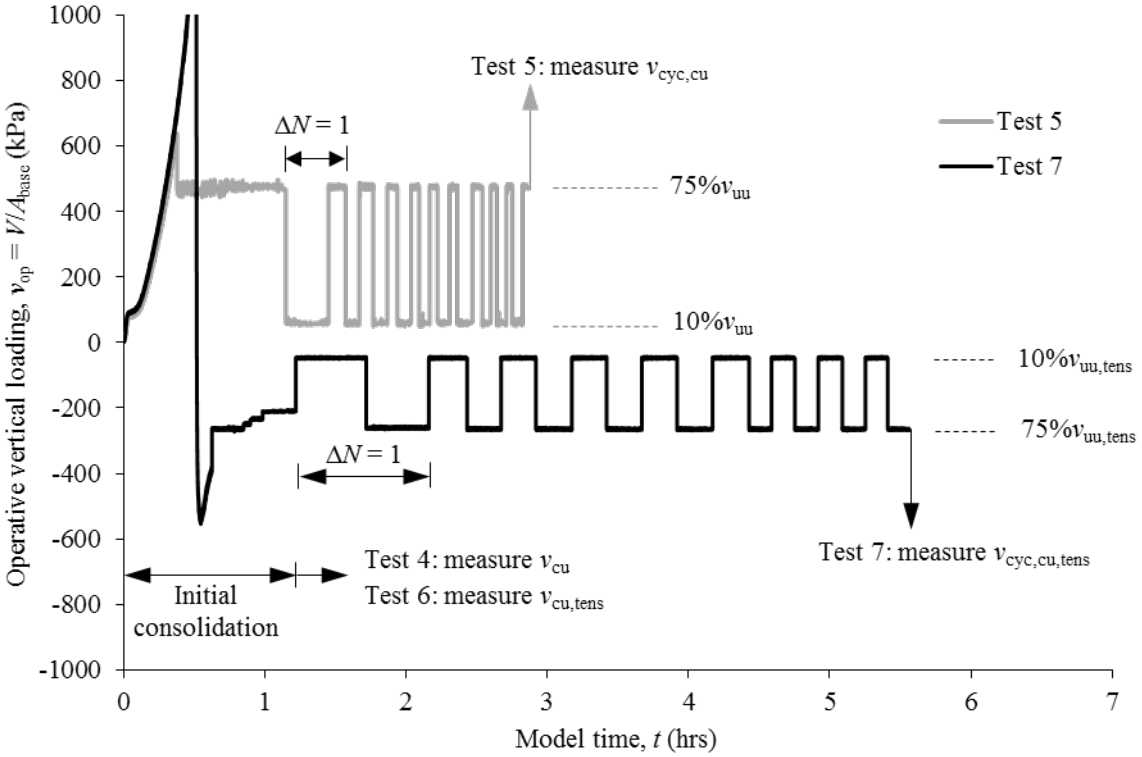

(c)

Figure 11 Time histories (at model scale) of (a) operative vertical loading, v_{op}, and overview of test procedures for surface model foundation tests (Test 1, 2 and 3); (b) operative horizontal loading, h_{op}, applied in Test 3; (c) operative vertical loading in embedded plate tests (Test 4 to 7)

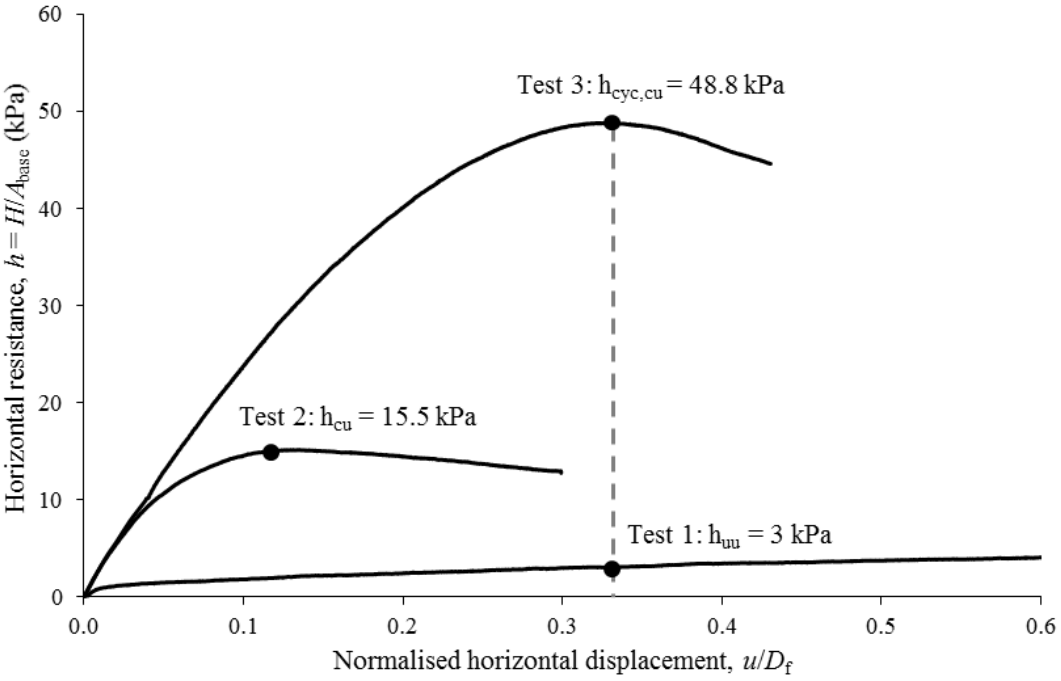

(a)

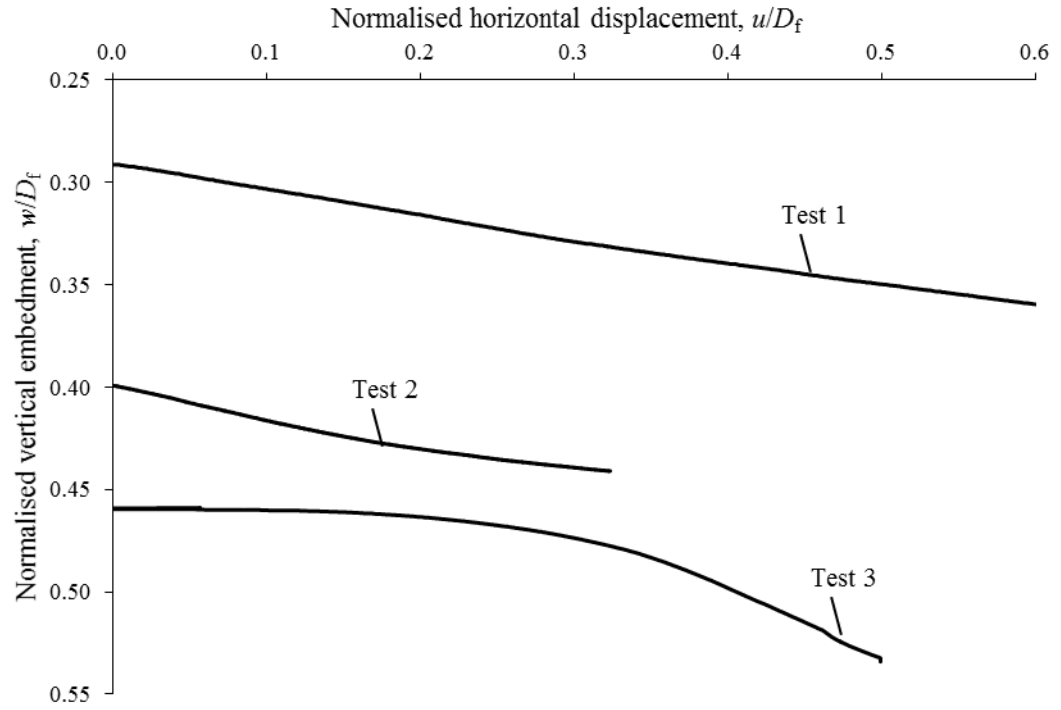

(b)

Figure 12 Responses during loading to failure (surface foundation tests): (a) horizontal resistance against normalised horizontal displacement, u/D_f; (b) trajectory

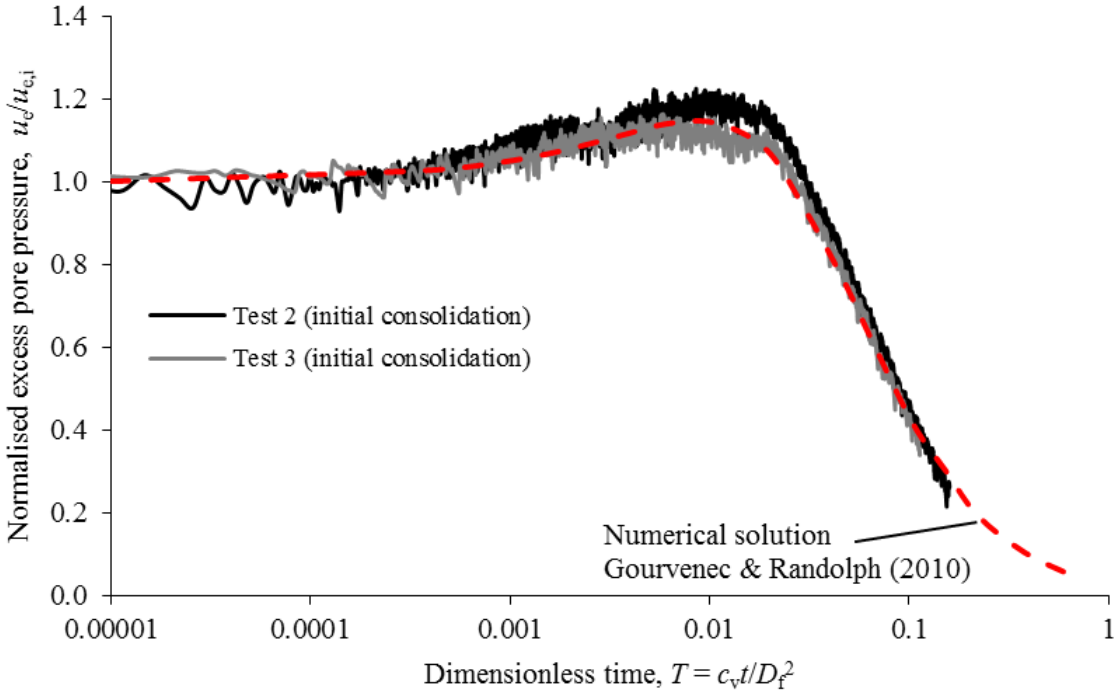

Figure 13 Dissipation response during initial consolidation (tests 2 and 3):

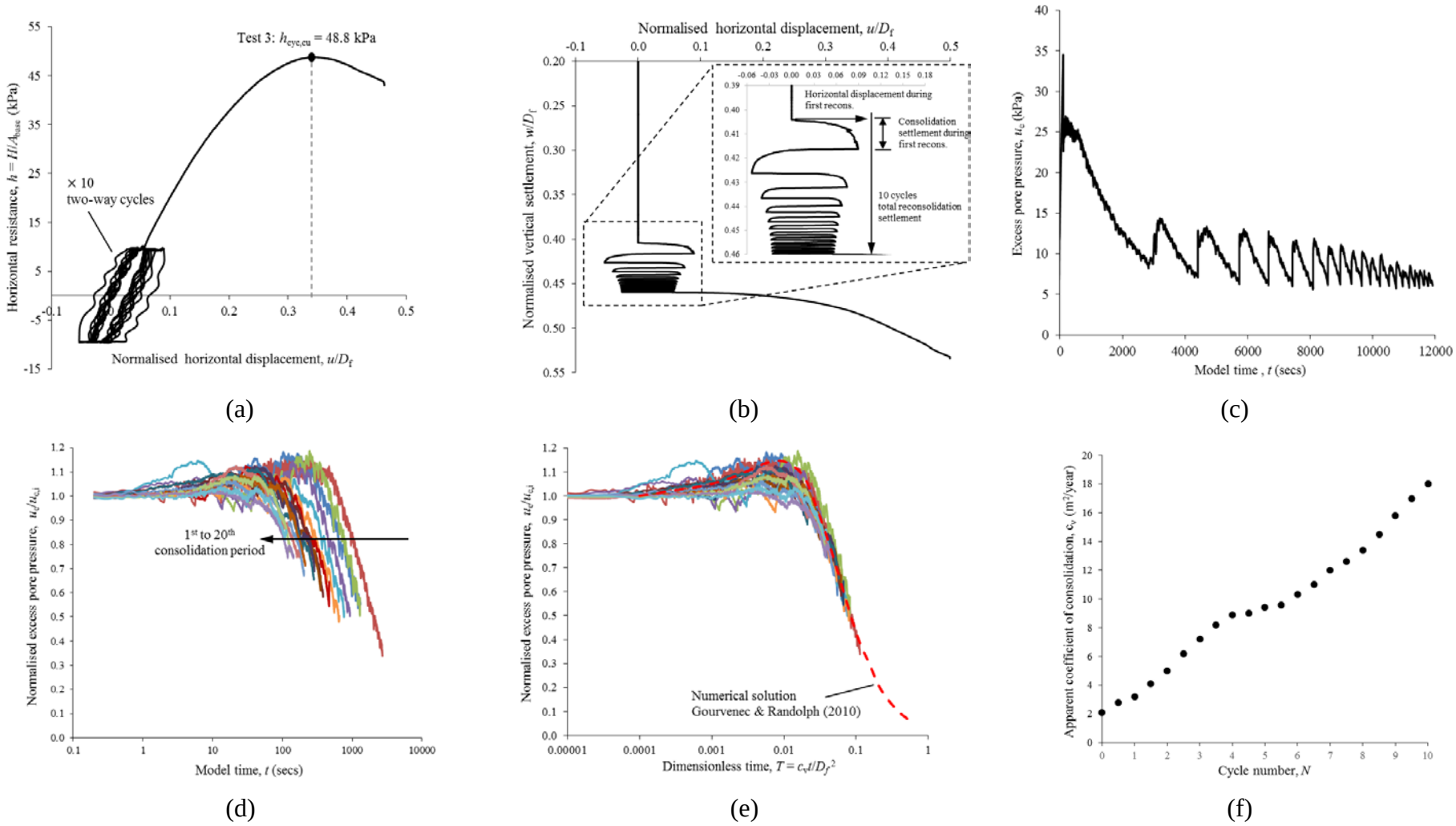

Figure 14 Shallow foundation (test 3): (a) horizontal load history; (b) settlement and horizontal displacement; (c) pore water pressure at foundation base throughout cyclic loading phases; (d) normalised excess pore pressure against time; (e) normalised excess pore pressure against dimensionless time; (f) apparent variation in coefficient of consolidation with cycles of consolidation

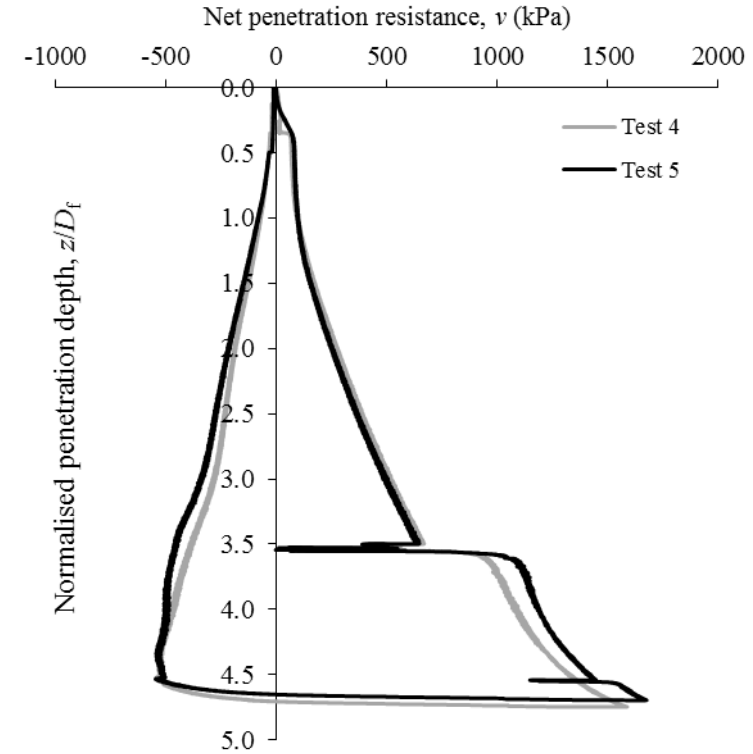

(a)

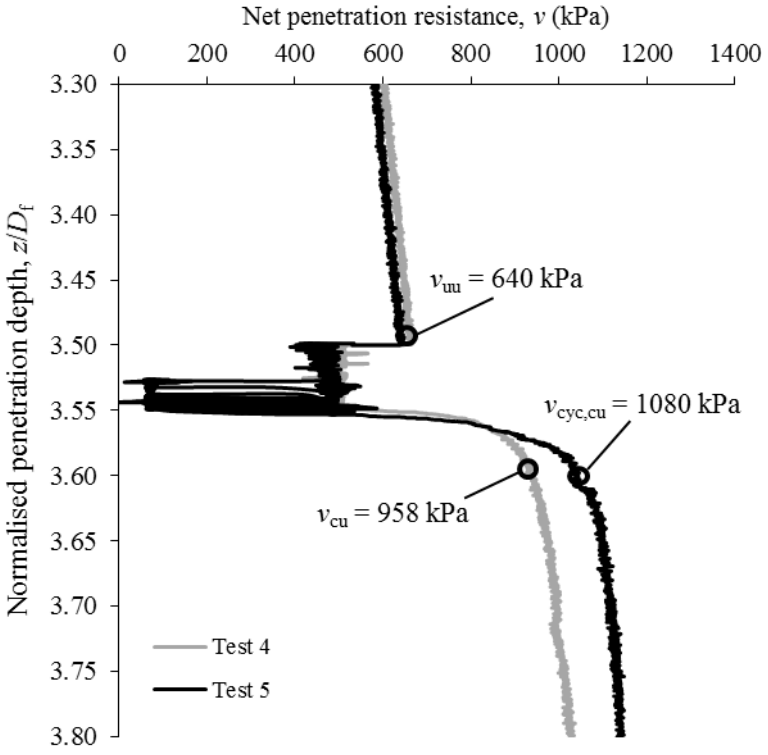

(b)

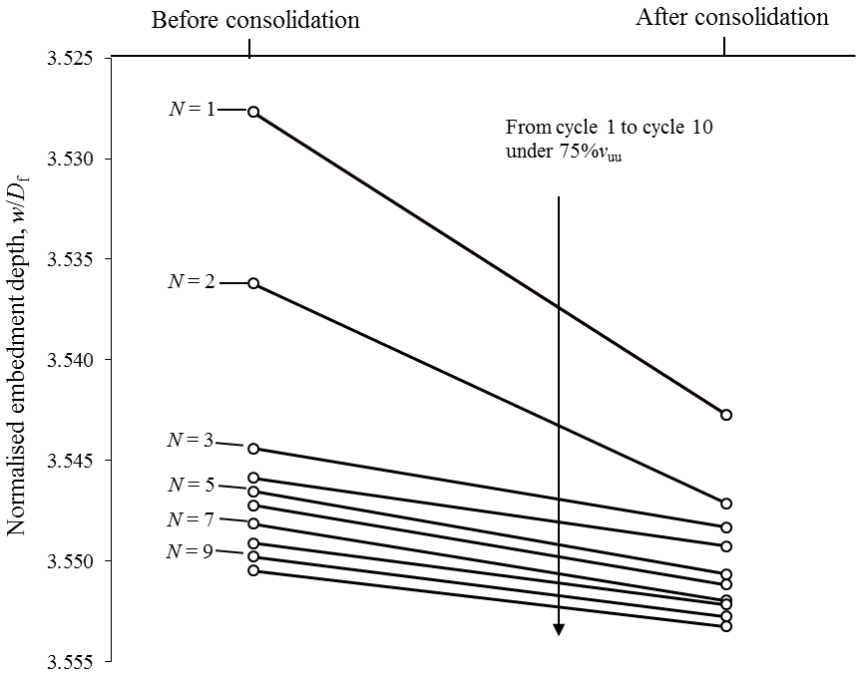

(c)

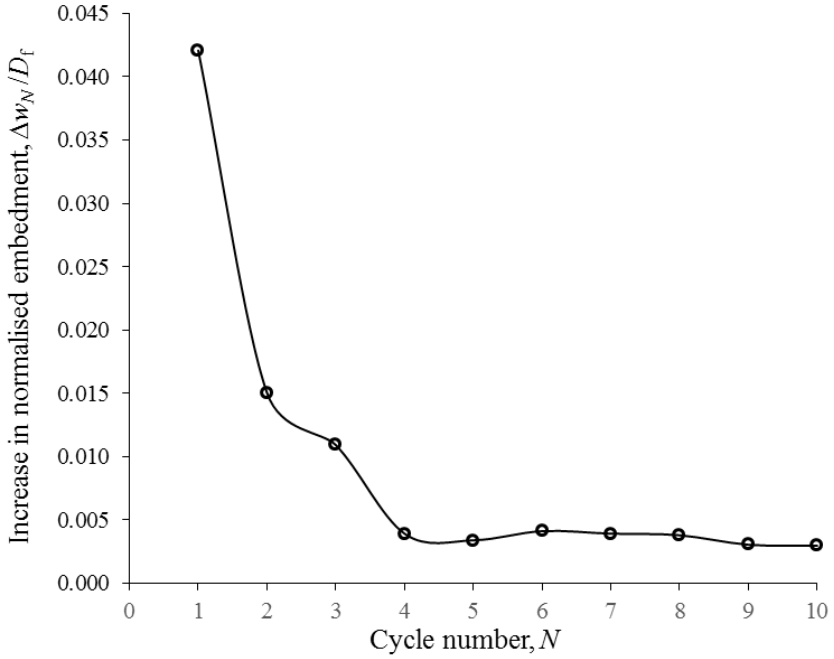

(d)

Figure 15 Buried plate compression tests (Test 4 and 5): (a) overall penetration resistance profiles; (b) sustained and cyclic loading phases; (c) consolidation settlement under sustained load (75%v_{uu}); (d) increase in normalised embedment through cycles under 75%v_{uu}

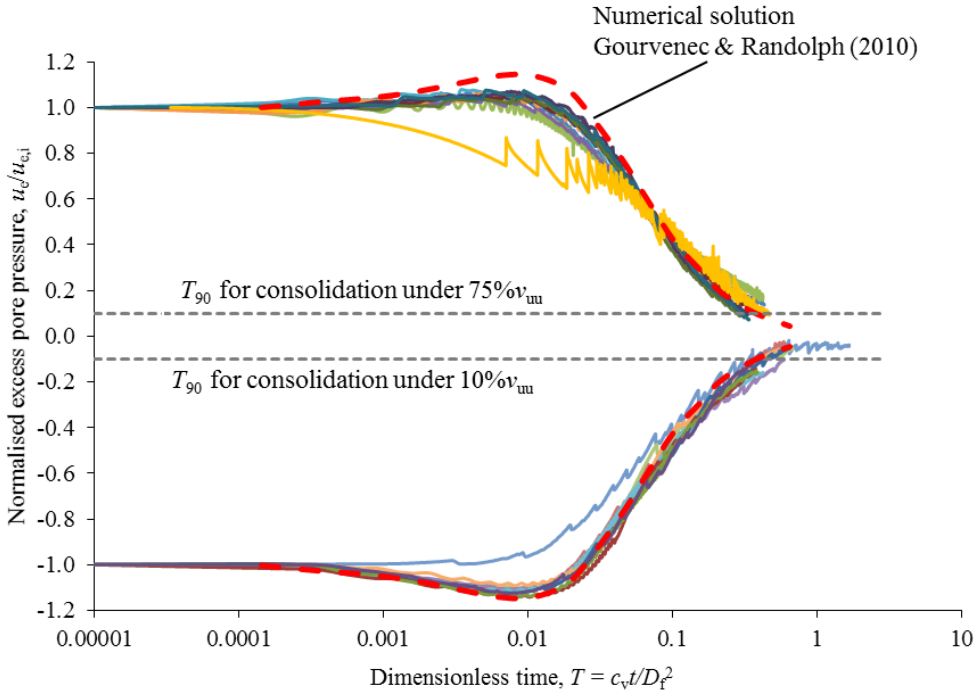

(a)

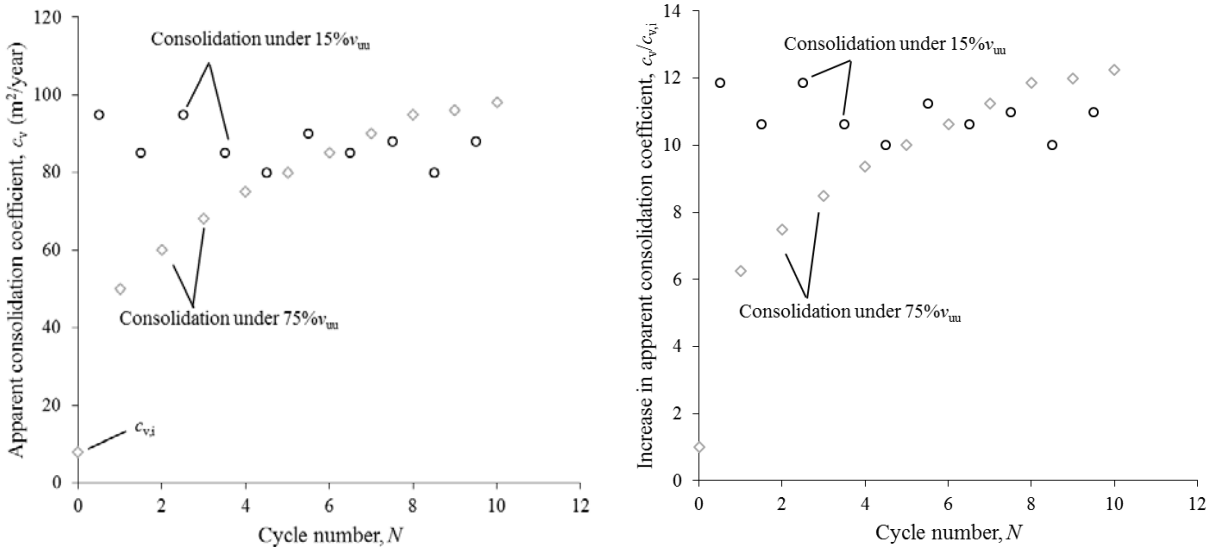

(b) (c)

Figure 16 Buried plate test 5: (a) normalised excess pore pressure dissipation; (b) variation in apparent consolidation coefficient, c_v; (c) proportional rise in an apparent consolidation coefficient, $c_v/c_{v,i}$

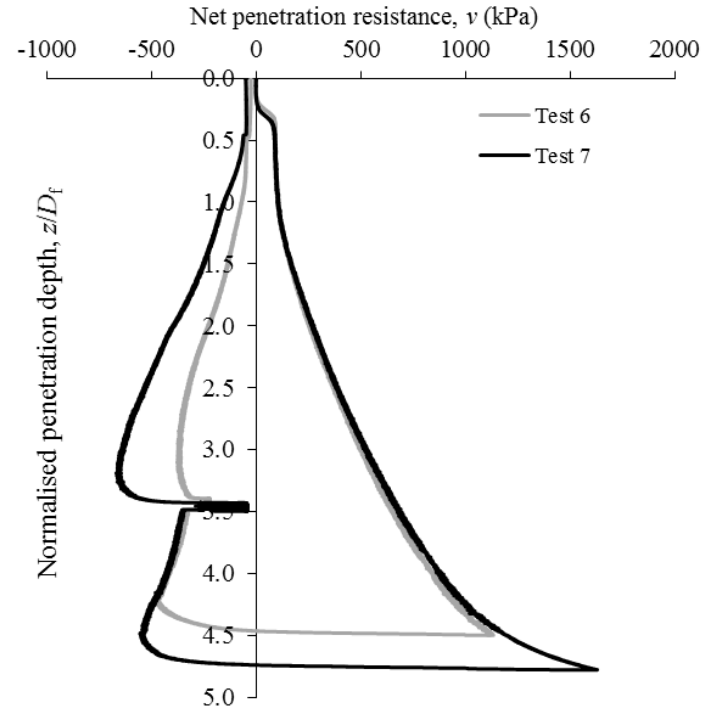

(a)

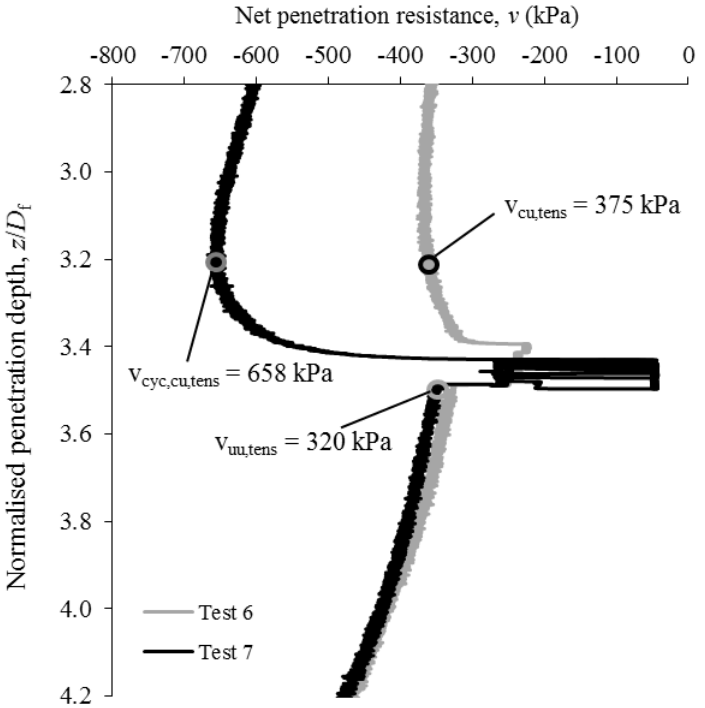

(b)

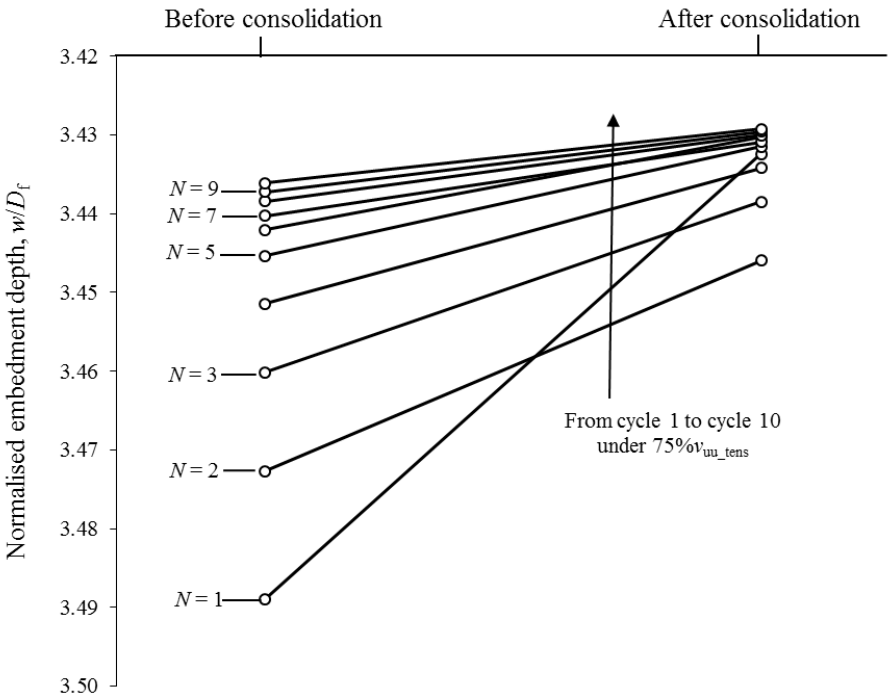

(c)

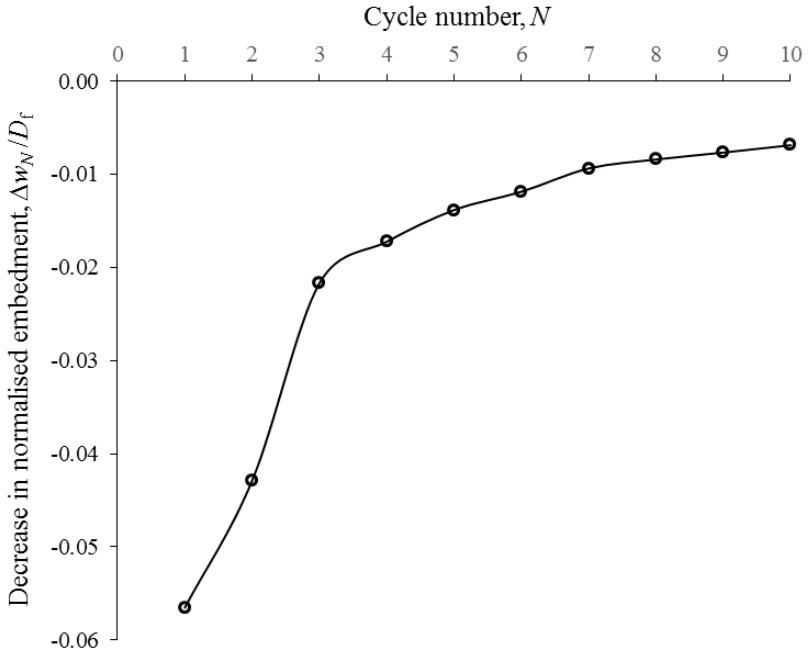

(d)

Figure 17 Buried plate tension tests (Test 6 and 7): (a) overall penetration resistance profiles; (b) sustained and cyclic loading phases; (c) consolidation settlement under sustained load ($75\%v_{uu,tens}$); (d) reduction normalised in embedment through cycles under $75\%v_{uu,tens}$

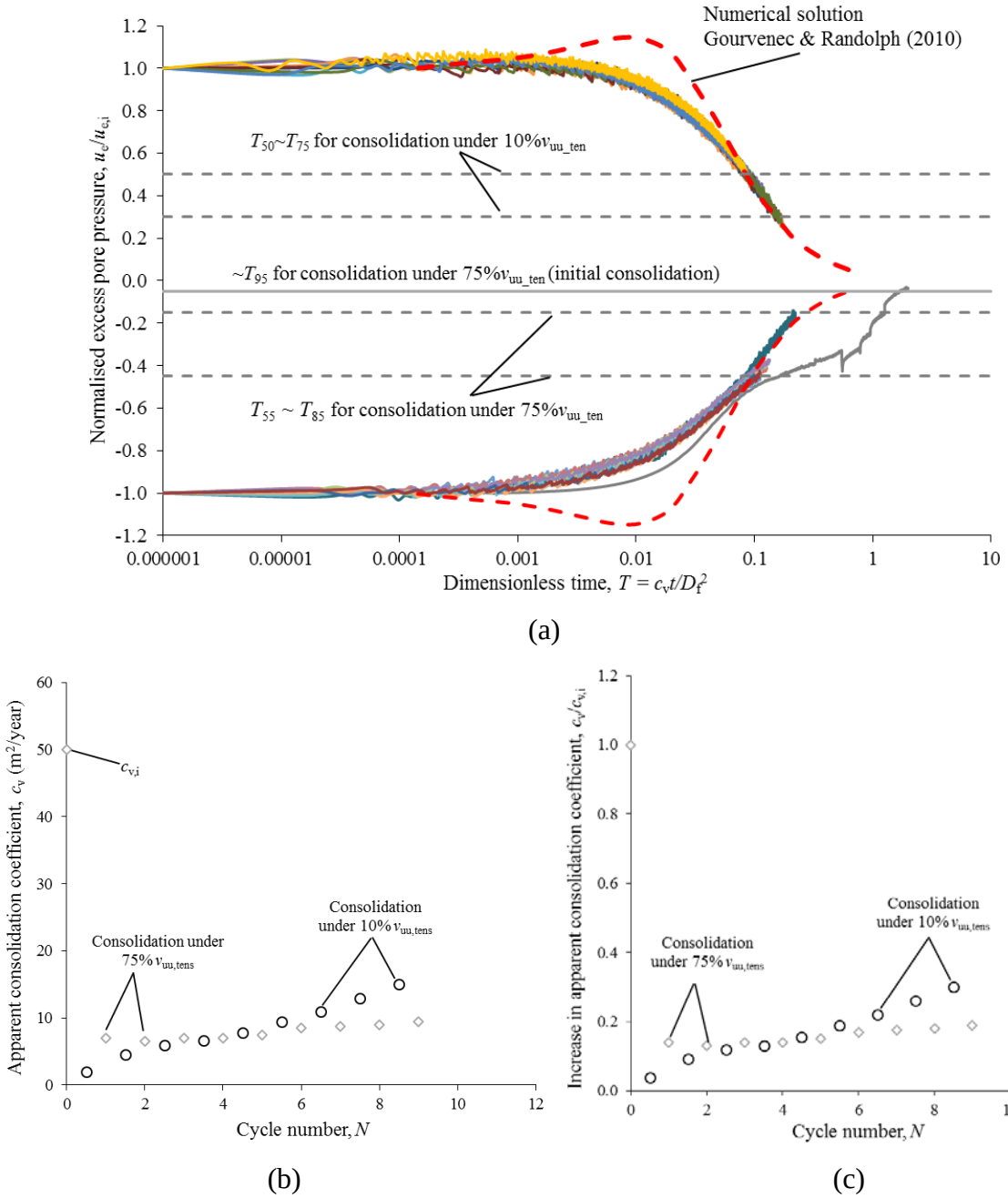

Figure 18 Buried plate test 5: (a) normalised excess pore pressure dissipation; (b) variation in apparent consolidation coefficient, c_v; (c) proportional rise in an apparent consolidation coefficient, $c_v/c_{v,i}$

Table 1 Geometric details of model foundation and penetrometers

			Model foundation	T-bar	Piezoball
Dimension	Diameter	(mm)	$D_f = 40$	$D_{T\text{-}bar} = 5$	$D_{PB} = 15$
	Length	(mm)	-	$L = 20$	-
	Thickness	(mm)	$t_f = 10$	-	-
	Shaft diameter	(mm)	$D_{shaft,f} = 10$	$D_{shaft,T\text{-}bar} = 5$	$D_{shaft,PB} = 5$
Instrumentation			Pore pressure transducer at centre of foundation invert	Tip load cell	Tip load cell Pore pressure transducer at mid face (0.25 diameters from the tip of the ball)

Table 2 Characteristics of the natural carbonate silt (Chow et al. 2019)

Parameter	**Unit**	**Value**
Liquid limit, *LL*	%	67
Plastic limit, *PL*	%	39
Specific gravity, G_s	(-)	2.71
Slope of normal compression line, λ	(-)	0.287
Slope of swelling line, κ	(-)	0.036
Poisson ratio, ν	(-)	0.32
Critical state frictional constant, *M*	(-)	1.62
Angle of internal friction, ϕ'	(°)	40

Table 3 Centrifuge test programme

Test type	Tests	Penetration velocity		**Remarks**
		v_p (mm/s)	v_pD/c_v	
Non-conventional penetrometer tests	Episodic[1] T-bar	3	118	T-bar: 78 cycles of penetration, extraction to mudline and waiting above mudline for 780 s
	Episodic cyclic piezoball	1	118	Piezoball: 3 episodes of cyclic penetration (20 cycles) at $4D_{PB}$ and $10.5D_{PB}$ with a rest period of reconsolidation between each episode
Foundation tests	Test 1 (surface foundation)	0.1	32	Immediate rapid failure: provides the undrained unconsolidated horizontal capacity, h_{uu}
	Test 2 (surface foundation)	0.1	32	Sustained vertical load with consolidation, followed by rapid failure: provides the consolidated undrained horizontal capacity, h_{cu}
	Test 3 (surface foundation)	0.1	32	10 cycles of horizontal loading to $\pm 0.75h_{cu}$ allowing time for pore pressure dissipation: provides the cyclic consolidated undrained horizontal capacity, $h_{cyc,cu}$
	Test 4 (embedded plate)	0.1	32	Penetration to depth of $z = 3.5D_f$, maintained loading (75% v_{uu}) with reconsolidation: provides unconsolidated undrained (v_{uu}) and consolidated undrained (v_{cu}) vertical capacity
	Test 5 (embedded plate)	0.1	32	Penetration to depth of $z = 3.5D_f$, episodic cyclic loading (10%-75% v_{uu}) with reconsolidations: provides cyclic consolidated undrained vertical capacity ($v_{cyc,cu}$)
	Test 6 (embedded plate)	0.1	32	Penetration to depth of $z = 3.5D_f$, maintained uplift loading (75% $v_{uu,tens}$) with reconsolidation: provides unconsolidated undrained ($v_{uu,tens}$) and consolidated undrained tensile capacity ($v_{cu,tens}$)
	Test 7 (embedded plate)	0.1	32	Penetration to depth of $z = 3.5D_f$, episodic cyclic loading (10%-75% $v_{uu,tens}$) with reconsolidations: provides cyclic consolidated undrained tensile capacity ($v_{cyc,cu,tens}$)

[1] Episodic: a test involving cyclic phases interspersed with pause periods (during which consolidation can occur)

Table 4 Procedures in horizontally-loaded shallow foundation tests

Test	Installation	Simulated 'operative loading history'	Failure stage
1	Undrained penetration (at 0.1 mm/s) to v_{op} ~ 22.5 kPa (reached at z/D_f ~ 0.3). Immediately followed by unloading to $2/3v_{op}$ which was maintained throughout the test including the failure stage, representing self-weight loading (e.g. Figure 11a)	Loaded immediately to failure	Displaced horizontally at 0.1 mm/s to record h_{uu}
2		Consolidated for ~70 mins under v_{op} (equivalent to T ~ 0.15 i.e. sufficient for ~80% pore pressure dissipation)	Displaced horizontally at 0.1 mm/s to record the consolidated undrained capacity, h_{cu}
3		Consolidated for ~50 mins (65% of excess pore pressure dissipated) under $2/3v_{op}$ then subjected to 10 cycles of horizontal loading to $\pm 75\% h_{cu.}$ The pore pressure dissipation period was varied, allowing ~45% of excess pore pressure to dissipate after each change in load for the first 5 cycles, reducing to ~25% for the later cycles (Figure 11b).	Displaced horizontally at 0.1 mm/s to record the cyclic consolidated undrained capacity, $h_{cyc,cu}$

Table 5 Procedures in vertically-loaded plate foundation tests

Test	Installation	Simulated 'operative loading history'	Failure stage
4	Undrained penetration (at 0.1 mm/s) to w/D_f ~ 3.5 (v_{uu} was taken as the capacity at this depth).	Consolidated under compression of ~$0.75v_{uu}$ until ~90% pore pressure dissipation (equivalent to T ~ 0.3)	Penetrated at 0.1 mm/s to record v_{cu}, then extracted at 0.1 mm/s
5		Subjected to 10 cycles of vertical compression loading between ~$0.1v_{uu}$ and ~$0.75v_{uu}$, with ~90% pore pressure dissipation after each change in load (i.e. 20 dissipations from 10 cycles)	Penetrated at 0.1 mm/s to record $v_{cyc,cu}$, then extracted at 0.1 mm/s

6	Undrained penetration (at 0.1 mm/s) to $w/D_f \sim 4.5$ followed by extraction to $w/D_f \sim 3.5$ ($v_{uu,tens}$ was taken as the capacity at this depth).	Consolidated under tension of ~0.75$v_{uu,tens}$ until ~95% pore pressure dissipation (equivalent to $T \sim 2$)	Extracted at 0.1 mm/s to record $v_{cu,tens}$
7		Subjected to 10 cycles of vertical tension loading between ~0.1$v_{uu,tens}$ and ~0.75$v_{uu,tens}$. Consolidation periods in the first cycle were 35 mins that are equivalent to ~95% and 50% dissipation, and the periods for cycle 2 to 6 were 15 mins, except for the third consolidation that was 26 mins. Subsequently, the consolidation periods in the last three cycles were 10 mins.	Extracted at 0.1 mm/s to record $v_{cyc,cu,tens}$

Table 6 Observed changes in foundation capacity from cyclic loading and consolidation

Test depth	Test ID	Foundation capacity, v or h (kPa)	Capacity ratio, h/h_{uu}, v/v_{uu} or $v/v_{uu,tens}$
Shallow ($<0.5D_f$)	Test 1	$h_{uu} = 3$	1
	Test 2	$h_{cu} = 15.5$	5.2
	Test 3	$h_{cyc,cu} = 48.8$	16.3
Deep ($3.5D_f$)	Test 4	$v_{uu} = 640$	1
		$v_{cu} = 958$	1.5
	Test 5	$v_{cyc,cu} = 1080$	1.7
	Test 6	$v_{uu,tens} = 320$	1
		$v_{cu,tens} = 375$	1.2
	Test 7	$v_{cyc,cu,tens} = 658$	2.1